Chemical Engineering Journal 393 (2020) 124726

Contents lists available at ScienceDirect

Chemical Engineering Journal

journal homepage: www.elsevier.com/locate/cej

Review

Recent progress in electrode fabrication for electrocatalytic hydrogen evolution reaction: A mini review

Wei Yang[a,*], Shaowei Chen[b,*]

[a] State Key Laboratory of Hydraulics and Mountain River Engineering, College of Water Resource & Hydropower, Sichuan University, Chengdu 610065, China
[b] Department of Chemistry and Biochemistry, University of California, 1156 High Street, Santa Cruz, CA 95064, USA

HIGHLIGHTS

- HER performance depends on electron transfer, proton diffusion and bubble release.
- A wide range of support materials.
- Critical substrate parameters include porosity, electrical conductivity, and chemical stability.
- Electrode fabrication by 3D printing.
- Superaerophobic surface.

GRAPHICAL ABSTRACT

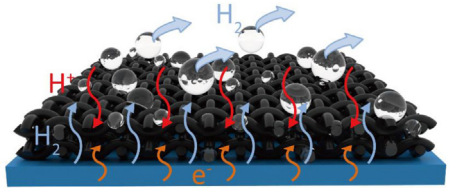

ARTICLE INFO

Keywords:
Hydrogen evolution reaction
Electrode
Ion diffusion
Superaerophobicity
Bubble release

ABSTRACT

Electrochemical hydrogen evolution reaction (HER) is of great importance for high-efficiency, low-cost production of hydrogen. As the HER activity of catalysts has been significantly improved in recent years, the routings from catalysts to electrodes represent a key step for practical HER applications. In an HER electrode, hydrogen reduction is accomplished by electron transfer, proton diffusion and bubble release. These processes should be taken into account in the design, engineering and fabrication of the electrode. In this review, we begin with a discussion of the correlation between these important issues and the overall electrochemical HER performance, and then summarize recent progress in the design and fabrication of HER electrodes, with a focus on the effects of electrode structure, electrolyte penetration, ion diffusion and bubble adhesion/release on the HER performance. We conclude with a perspective of strategies for further enhancement and the critical challenges for HER electrode fabrication.

1. Introduction

Development of renewable energy conversion and storage technologies has been hailed as a viable strategy to reduce our dependence on fossil fuels, such as coal and gasoline, and the emissions of waste gases such as carbon dioxide, sulfur dioxide and nitrogen oxides [1–3]. Hydrogen, as a clean energy carrier with a high energy density, has been generally recognized as a promising alternative to fossil fuels [4–7]. To this end, hydrogen evolution reaction (HER) in water electrolysis has been attracting extensive attention, where high-purity hydrogen is produced under ambient conditions. HER primarily involves two routes, the Volmer–Tafel pathway, and the Volmer–Heyrovsky pathway [8]. The HER efficiency is significantly dependent on the selection of catalysts. Currently, platinum and ruthenium oxide-based materials are the catalysts of choice for HER in both acid and base media [9–11], but high costs, limited availability and natural scarcity have hindered their wide-spread applications.

Thus, significant efforts have been devoted to the development of high-efficiency HER catalysts based on earth-abundant, cost-effective materials. Among these, transition metal sulfides, phosphides, oxides, carbides and nitrides have been found to demonstrate high catalytic activities towards HER [12–17]. For example, Tian et al. [18] reported

* Corresponding authors.
E-mail addresses: wei_yang@scu.edu.cn (W. Yang), shaowei@ucsc.edu (S. Chen).

https://doi.org/10.1016/j.cej.2020.124726
Received 1 November 2019; Received in revised form 5 March 2020; Accepted 8 March 2020
Available online 09 March 2020
1385-8947/

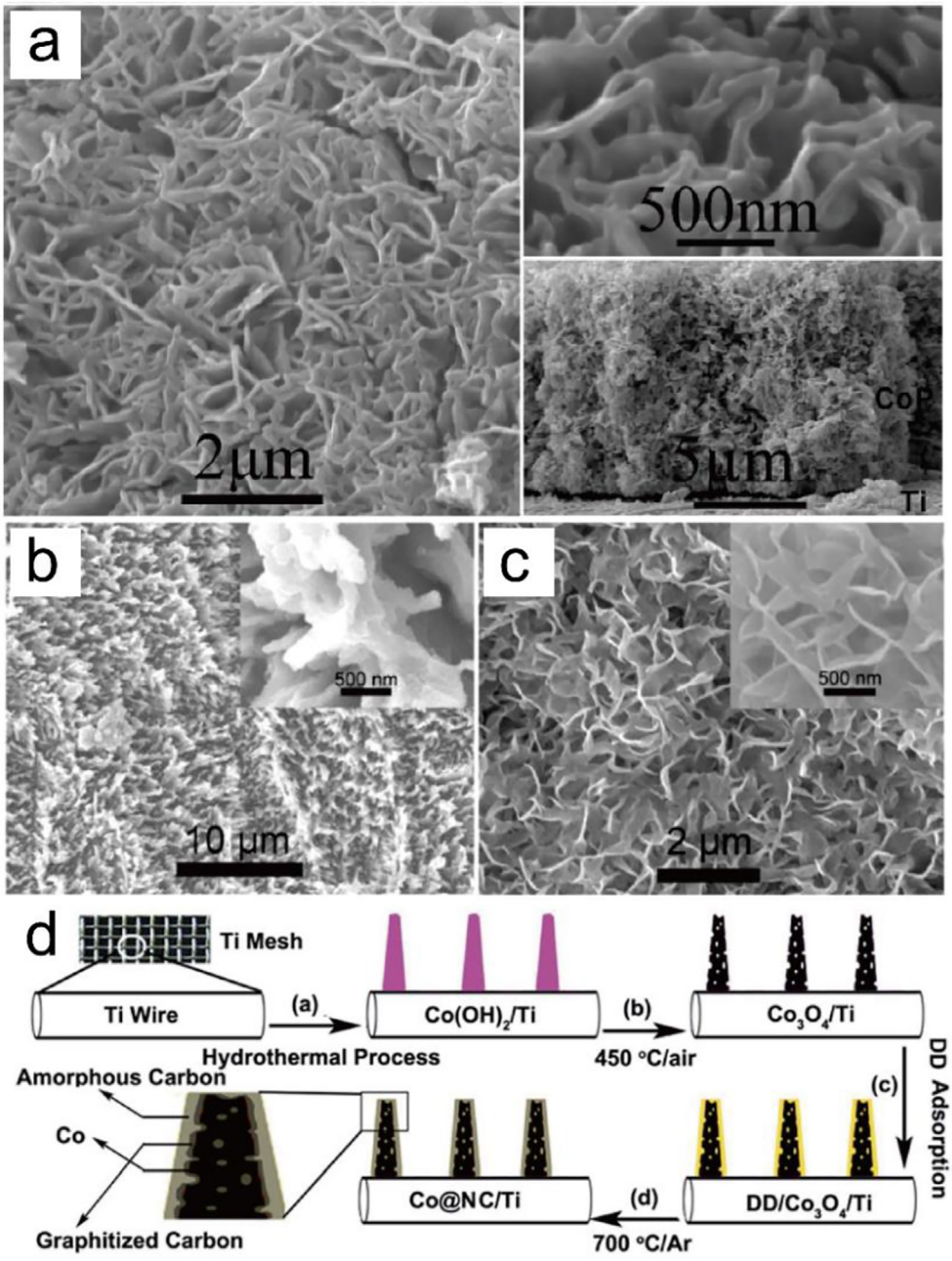

Fig. 1. SEM images of (a) CoP/Ti electrode, (b) Ti plate and (c) MoS_2 NAs/Ti electrode. Insets to panels (b, c) are the corresponding high-resolution images. Panel (a) reproduced with permission from Ref. [42] © American Chemical Society. Panels (b, c) reproduced with permission from Ref. [44] © Elsevier. (d) Schematic of the synthesis of Co@NC/Ti. Panels (d) reproduced with permission from Ref. [40] © Elsevier.

that self-supported nanoporous cobalt phosphide nanowire arrays can serve as highly efficient HER catalysts, which exhibited a low overpotential (η_{10}) of -67 mV to reach the current density of 10 mA cm^{-2} (close to that of Pt). Similarly, Liang et al. [19] prepared iron phosphide nanorod arrays as cost-effective HER catalysts, with a lower η_{10} of -58 mV in 0.5 M H_2SO_4. As the intrinsic activity of such catalysts has been significantly improved in the past decades, current efforts have been devoted to implementing these catalysts for HER applications through electrode design and fabrication.

Traditional HER electrodes are fabricated by coating a layer of active materials on the electrode surface, which should be chemically stable and electrically conductive. The active materials and the substrate serve as a porous layer for HER catalysis and as a current collector, respectively [20]. In the electrode, there are three major processes during HER, electron transfer, proton diffusion and bubble release, that largely dictate the HER performance. Therefore, the fabrication of an effective HER electrode should satisfy three principles. First, the catalysts used should possess a high intrinsic electrocatalytic activity, which can facilitate electron transfer between protons and electrode. Second, the electrode (and catalyst) should have a highly porous structure, which can provide sufficient channels for proton diffusion and bubble transport inside the electrode. Third, the electrode surface should promote the release of hydrogen bubbles, since bubbles can block ion diffusion and reduce the effective surface area of the electrode. With an abundant pore structure and high electrical conductivity, nickel foam, carbon cloth, graphene film, graphene aerogel, carbon aerogel, and carbon felt have been used rather extensively as electrode substrates [21–26]. For instance, Shi et al. prepared an HER electrode based on $MoSe_2$ supported on graphene-carbon nanotube aerogel (GCA-$MoSe_2$), and found that GCA significantly reduced the

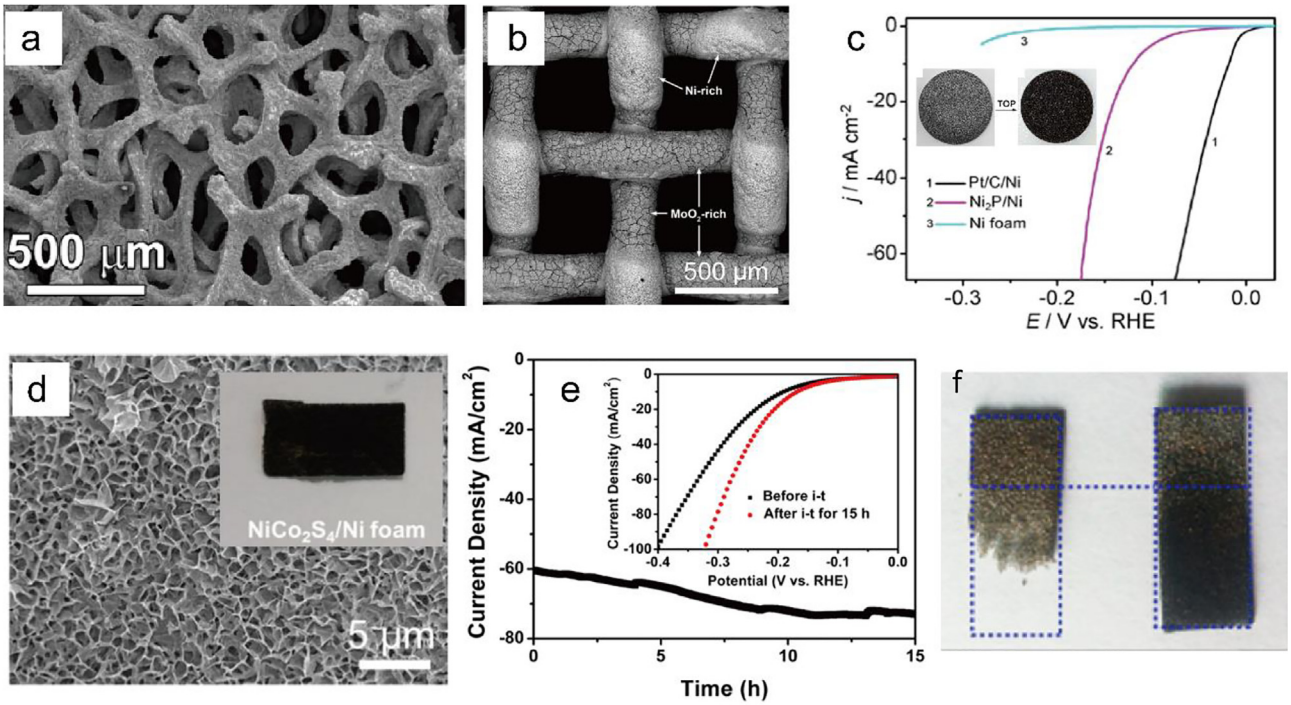

Fig. 2. (a) SEM image of a nickel foam. Panel (a) reproduced with permission from Ref. [48] © American Chemical Society. (b) SEM image of a nickel mesh. Panel (b) reproduced with permission from Ref. [49] © Elsevier. (c) Polarization curves of Ni_2P/Ni, Pt/C/Ni, and bare Ni foam at the potential scan rate of 5 mV s^{-1} in 0.5 M H_2SO_4. Insets are the photographs of the bare Ni foam before (left) and after (right) being treated with TOP at elevated temperature. Panel (c) reproduced with permission from Ref. [56] © American Chemical Society. (d) SEM image of the NiCo-LDH/Ni foam. Inset is the corresponding photograph of the NiCo-LDH/Ni foam. Panel (d) reproduced with permission from Ref. [59] © Elsevier. (e) Current–time plots of Ni foam electrode at the applied potential of −0.43 V (vs RHE) in 0.5 M H_2SO_4 for up to 15 h. Inset are the corresponding polarization curves before and after 15 h's continuous operation. (f) Photographs of the Ni foam (left) dipped in 0.5 M H_2SO_4 solution for 15 h and (right) after i–*t* test at −0.43 V vs RHE in 0.5 M H_2SO_4 for 15 h. Panels (e, f) reproduced with permission from Ref. [60] © American Chemical Society.

onset potential (E_{onset}) from −198 to −113 mV vs. RHE, and η_{10} from −297 to −228 mV in 0.5 M H_2SO_4, as ion/electrolyte transport at electrode interface was facilitated [27].

Notably, high-efficiency catalysts alone are not sufficient in the fabrication of an HER electrode, as the contact between the electrode and electrolyte can be hindered by the adhesion of hydrogen bubbles on the electrode surface, resulting in an increase of ohmic drop and a decrease of HER efficiency [28,29]. For example, in the evaluation of the HER performance of a cathode at the constant potential of −0.3 V vs. RHE, Hou et al. [30] observed a fluctuation of the HER current that was closely related with the accumulation and release of H_2 bubbles on the electrode surface. Similarly, Perera et al. [31] investigated the dynamic behaviors of hydrogen bubbles and found that the transient current response was dominated by the bubble nucleation, growth, and release. To minimize the detrimental effect induced by H_2 bubbles, the concept of "superaerophobic" surface has been introduced for HER electrode design. Several studies have shown that a "superaerophobic" surface can be constructed by changing the three-phase contact line (TPCL), which is crucial for the interactions between H_2 bubbles and solid surfaces [28,29,32,33]. In this design, the TPCL can be adjusted by controlling the nanostructures on the electrode surface during electrode fabrication, which effectively diminishes the adhesion force of bubbles and improves the HER performance. Although a number of remarkable catalysts and electrodes with "superaerophobic" surfaces have been developed, the evolution from catalysts to electrodes needs further exploration.

Prior reviews have mainly focused on the studies of the catalyst materials, analysis of the catalytic mechanism and electrocatalytic activity [34–38]. Yet, reports of the fabrication of HER electrodes have been scarce. In this review we will first discuss the relationship between electrode structure, bubble adhesion/release, electrolyte penetration, ion diffusion and HER performance of the electrode, summarize recent progress in the design and fabrication of HER electrodes, describe approaches to further improve the electrode performance, and finally include a prospective of the critical challenges for HER electrode design.

2. Transition metal-based electrodes

2.1. Titanium plate/mesh-based electrodes

Because of excellent electrical conductivity and high corrosion resistance to acid and alkaline media, titanium plates have been chosen as electrode substrates and current collectors in recent studies [39–41]. To prepare HER electrodes, a layer of catalysts is usually coated on the surface of a Ti plate, such as CoP nanosheet arrays, Ni_2P nanoparticles, FeP nanoparticles/nanorods, $CoSe_2$ nanosheets, and MoS_2 nanosheets [39,42–46]. For example, Pu et al. [42] grew a CoP nanosheet array onto a Ti plate by electrodeposition at room temperature, which was then subject to low-temperature phosphidation. The as-prepared HER electrode exhibited an E_{onset} of −40 mV vs. RHE and η_{10} of −90 mV in 0.5 M H_2SO_4 (Fig. 1a). Similarly, Shi et al. [44] prepared an HER electrode by depositing a layer of MoS_2 nanosheet arrays onto a Ti plate (MoS_2 NAs/Ti) through a simple hydrothermal and calcination process, which displayed a small E_{onset} of −90 mV, and η_{10} of −108 mV in 0.5 M H_2SO_4 (Fig. 1b, c). The MoS_2 NAs/Ti electrode also exhibited high stability with a negligible loss of current density during continuous cyclic voltammetric and chronoamperometric tests.

Although a high catalytic activity is generally observed by coating a layer of nanostructured catalysts on the metal plate surface, it should be pointed out that the plate electrode is not conducive to mass transport (e.g., ion diffusion and bubble release). According to the principles of

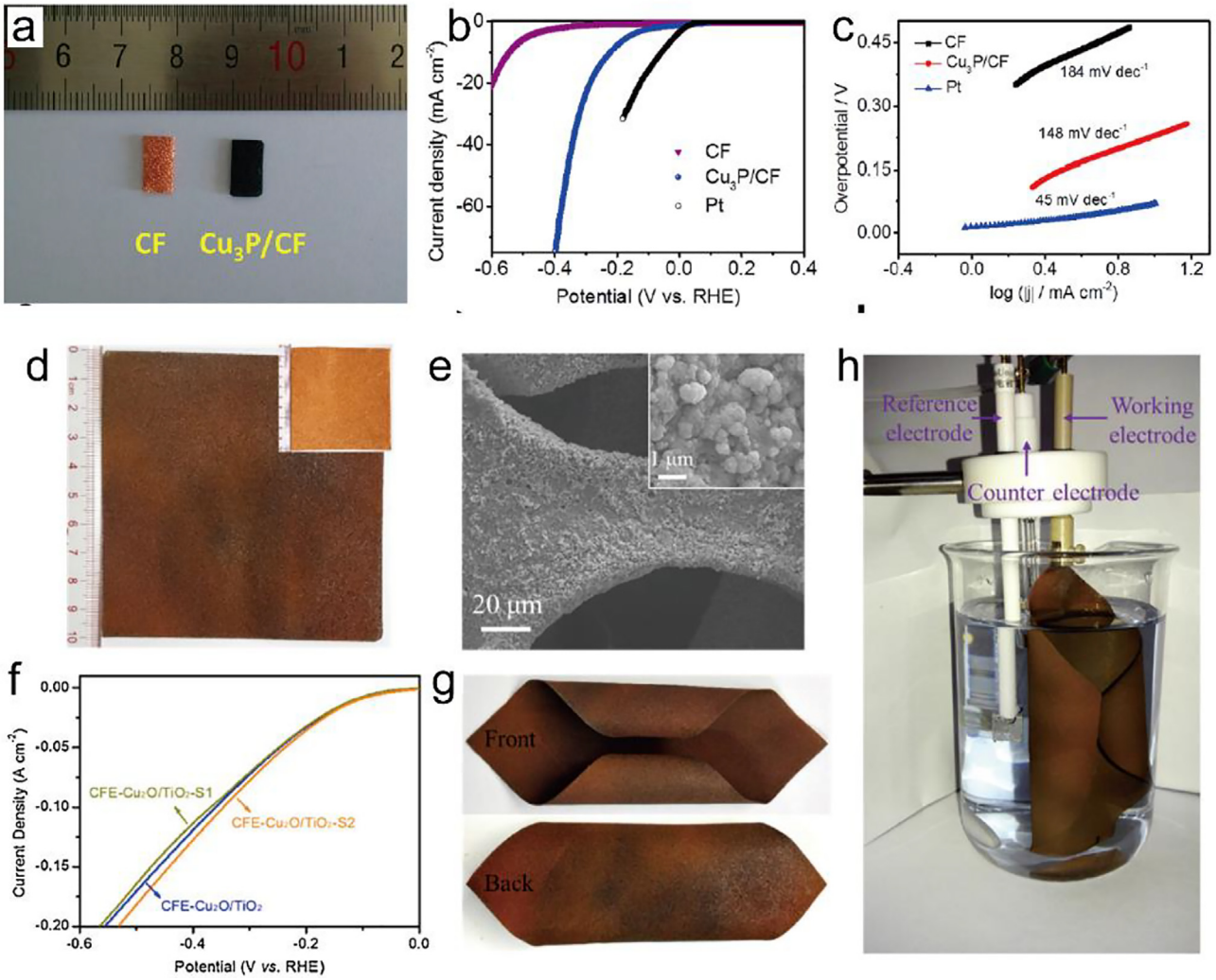

Fig. 3. (a) Photograph of blank CF (left) and Cu_3P/CF (right), (b) polarization curves and (c) the corresponding Tafel plots of Cu_3P/CF, CF, and commercial Pt. Panels (a-c) reproduced with permission from Ref. [61] © American Chemical Society. (d) Digital photograph and (e) SEM image of the as-prepared Cu_3P/CF electrode (the corresponding insets are of the untreated CF). (f) Polarization curves of the Cu_3P/CF electrode, (g) digital photograph of the Cu_3P/CF electrode bended into a specific shape, and (h) digital photograph of a HER set up in 1 M KOH using the Cu_3P/CF as the working electrode, Pt as the counter electrode and Ag/AgCl as the reference electrode. Panels (d-h) reproduced with permission from Ref. [62] © Elsevier.

electrode design, proton supply and bubble release can dominate the HER process. In a computational study based on finite elements simulation methods, Carneiro-Neto et al. [47] investigated the pH change at the electrode–electrolyte interface during HER, which was closely related to the current density. They found that the interfacial pH was 2–3 units higher than that in the bulk solution. This indicates that the H^+ concentration was 2–3 orders of magnitude lower near the electrode surface, corresponding to a 118–177 mV overpotential according to the Nernst equation. Therefore, to alleviate the limitation of ion diffusion and bubble releasing, titanium meshes have been used instead as alternative substrates for HER electrodes due to its porous structure. For example, in a recent study [40], N-doped carbon-encapsulated cobalt nanorod arrays were grown on a titanium mesh (Co@NC/Ti) as a HER electrode by a two-step procedure involving hydrothermal synthesis of Co_3O_4 nanorods followed by thermal reduction to metallic cobalt (Fig. 1d). The obtained Co@NC/Ti electrode exhibited an E_{onset} of −56 mV, which was close to that of commercial Pt/C (−12 mV); and the current densities increased sharply by 10 folds from 10 to 100 mA cm^{-2} when the Co@NC/Ti electrode potential was swept by less than 80 mV from −106 mV to −184 mV.

2.2. Nickel foam/mesh-based electrodes

Nickel foam/mesh has also been used extensively as an electrode substrate for HER electrodes (Fig. 2a and b), due to its excellent electrical conductivity, three-dimensional cross-linked network and hierarchical porous structure [48–50]. In addition, active materials in the forms of nanowires, nanoparticles, nanoflakes and nanorods can be in situ synthesized on the surface of nickel foam/mesh, such as nickel phosphides (Ni_2P) [51], nickel sulfide (Ni_3S_2) [52] and nickel alloys (such as Ni-B, Ni-Mo) [53,54] by chemical vapor deposition, hydrothermal treatment, low temperature phosphidation, and electrodeposition, which minimizes deactivation resulting from the reversible formation of nickel hydride species under alkaline condition [55]. Notably, a polymer binder is not needed when catalysts are directly in situ grown on the skeleton of nickel foam/mesh, minimizing the overpotential loss that arises from the block of active sites, the inhibition of ion diffusion, and the electrocatalyst/electrode interfacial resistance [51]. For instance, Shi et al. [56] prepared a Ni_2P nanosheets/Ni foam composite electrode through a facile chemical conversion pathway by using surface-oxidized Ni foam as a precursor and low concentration of trioctylphosphine as a phosphorus source, and the obtained Ni_2P/Ni electrode exhibited an improved HER performance with an E_{onset} of ca.

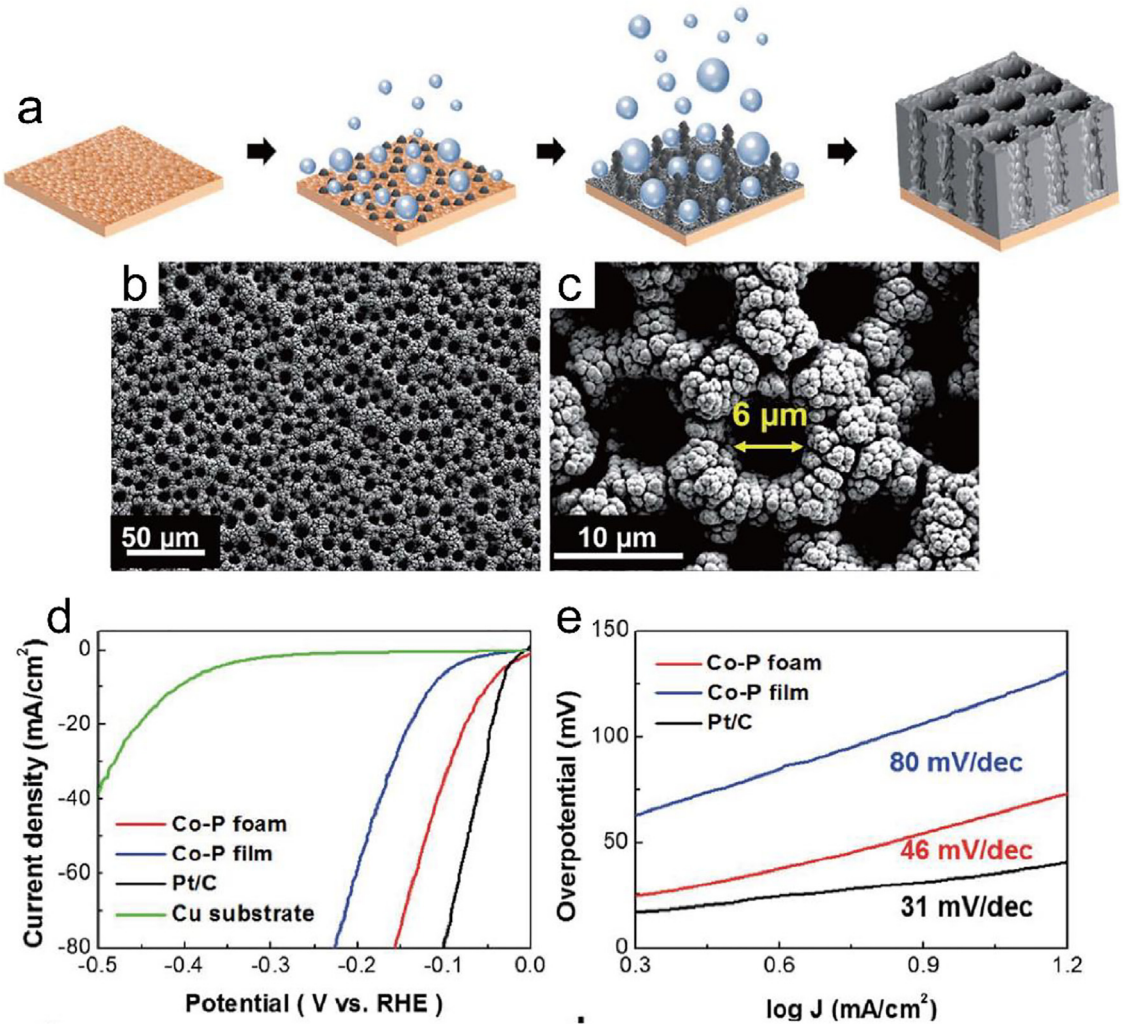

Fig. 4. (a) Schematic illustration of the synthesis of the Co–P foam, (b, c) SEM images of the Co–P foam at varied magnifications, (d) polarization and (e) Tafel curves of Co–P foam, Co–P film, Pt/C and Cu substrate. Reproduced with permission from Ref. [64] © Royal Society of Chemistry.

−80 mV in acid, significantly better than that of bare Ni foam (Fig. 2c).

In addition to nickel phosphides and nickel alloys, other transition metal sulfides and phosphides, such as CoP [57], FeP [20], MoS_2 [58], have also been used as active materials anchored on the surface of nickel foam substrates to improve the HER activity and durability of the electrode. For example, Ma et al. [59] prepared a $NiCo_2S_4$/Ni foam electrode by growing a layer of ultrathin $NiCo_2S_4$ nanoflakes onto the surface (Fig. 2d), and the electrode exhibited a low E_{onset} of −17 mV and long cycling stability (100,000 s) in alkaline solution. Nevertheless, the sustainability of nickel-based electrodes in acidic solutions remains challenging, because of easy dissolution of nickel by acid. To mitigate this issue, Lu et al. [60] described an effective method to stabilize the electrode by applying an overpotential as compared to the equilibrium potential of Ni^0/Ni^{2+} to the HER electrode, and the resulting nickel foam electrode exhibited an excellent and stable HER activity with an E_{onset} of −84 mV, η_{10} of −210 mV, and prominent electrochemical durability (> 5 d) in acidic electrolyte (Fig. 2e, f).

2.3. Copper foam/mesh-based electrodes

In comparison to nickel foam/mesh, copper foam/mesh has a lower cost and higher electrical conductivity, and thus is a highly favorable material as a HER electrode substrate. However, due to the low electrocatalytic activity of the copper foam substrate, a layer of catalytically active materials, such as Cu/Cu_2O nanowires, NiCoP@Cu_3P forests, CuN nanotubes and Cu_3P nanoarrays, has been anchored on the surface of copper foam through chemical or electrochemical methods, e.g., chemical oxidation, calcination and sequential phosphidation, and electrodeposition [61,63]. For example, Yu et al. [63] prepared Cu nanowires coated with FeNi layered double hydroxide nanosheets on a copper foam, which involved a chemical oxidation process to produce $Cu(OH)_2$ nanowires on the copper foam, transformation to CuO nanowires by calcination, and electrochemical deposition of FeNi layered double hydroxide nanosheets onto the nanowires. To simplify the preparation procedure, Hou et al. [61] fabricated an HER electrode by directly phosphatizing the copper foam at 300 °C using NaH_2PO_2 to form a layer of semimetallic Cu_3P nanoarrays. However, despite an apparent improvement of the HER performance, the as-prepared electrode exhibited a relatively high η_{10} of −222 mV in alkaline media, much larger than that of commercial Pt/C (−57 mV) (Fig. 3a–c). Interestingly, Long et al. [62] prepared a copper foam electrode decorated with a Cu_2O/TiO_2 composite through a facile etch and heat treatment, and the obtained electrode achieved a low η_{10} of −114 mV in alkaline media without iR correction (only slightly weaker than that of a Pt mesh (η_{10} = −82 mV). Scale-up experiments further demonstrated the feasibility in large-scale preparation of this electrode (Fig. 3d–h). More importantly, the as-prepared electrode even delivered an improved HER performance after the stability tests, probably due to the formation of Cu_2O/TiO_2 heterojunctions which facilitated electron transfer from Cu_2O to TiO_2 and hence led to enhanced HER on TiO_2.

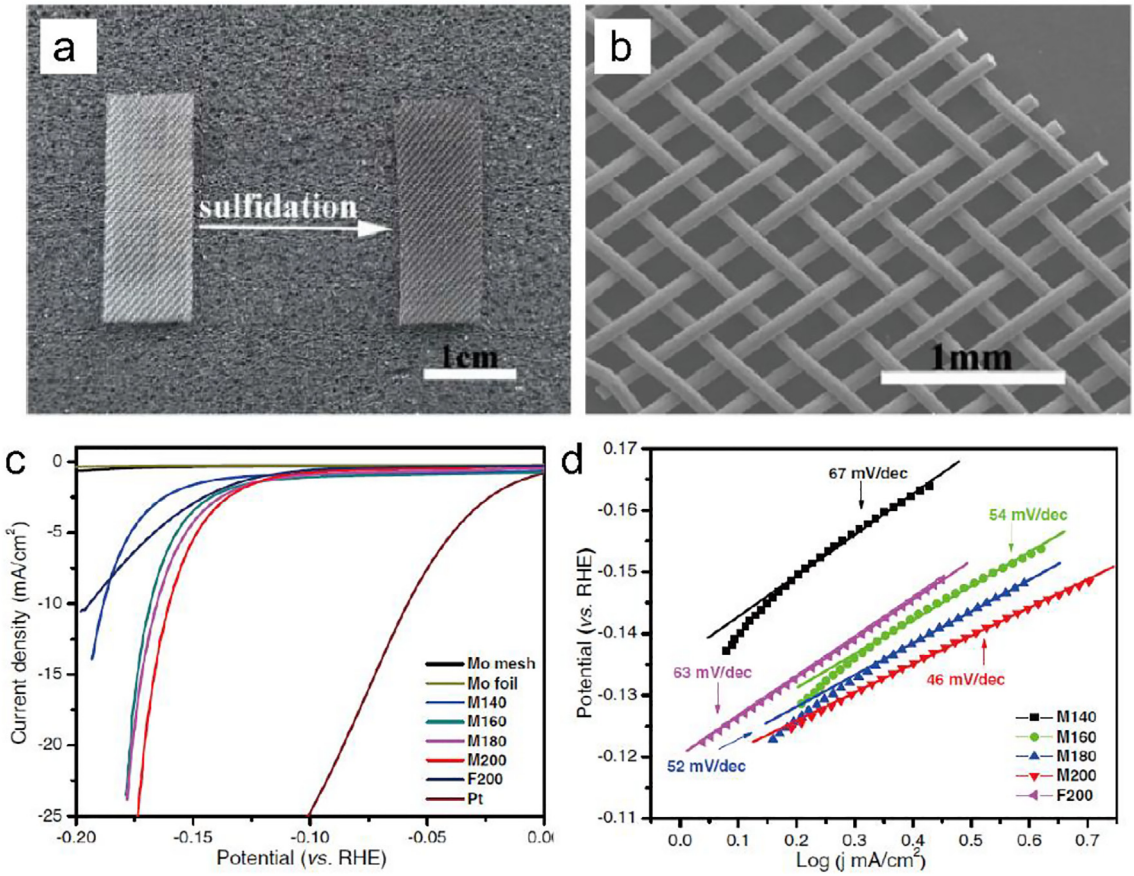

Fig. 5. (a) Photograph of a Mo mesh before (left) and after (right) hydrothermal treatment in aqueous thiourea solution, (b) SEM image of the Mo mesh, (c) polarization curves and (d) the corresponding Tafel plots for the Mo mesh-based electrodes. Reproduced with permission from Ref. [65] © Elsevier.

In addition to chemical oxidation, calcination and low temperature phosphidation, electrodeposition at a high current density is also a facile approach to the preparation of porous HER electrodes. For example, Oh et al. [64] prepared forest-like NiCoP@Cu_3P supported on a copper foam for HER by electrodeposition at the applied cathodic current density of 3 A cm^{-2}. During the electrodeposition process, the high current density induced fast deposition of Co and P on the substrate, and the rapidly generated hydrogen bubbles acted as a dynamic template for the skeleton Co–P structure by inhibiting the deposition of Co–P on the substrate surface, eventually leading to the formation of a highly porous Co–P foam structure (Fig. 4a–c). The as-prepared electrode exhibited a low η_{10} of −50 mV in 0.5 M H_2SO_4 and −131 mV in 1 M KOH, comparable to those of commercial Pt/C (–33 mV in 0.5 M H_2SO_4, and −80 mV in 1 M KOH). In addition, the electrode also showed high stability with a small increase of η_{10} from −50 to −63 mV after 2000 cycles.

Taken together, these studies demonstrated the feasibility of the fabrication of highly efficient HER electrode based on copper foam. However, it should be noticed that the corrosion resistance of copper foam/mesh is generally lower than that of nickel metal; thus the sustainability of copper foam/mesh as HER electrodes needs to be further improved.

2.4. Other metal-based electrodes

In addition to the materials discussed above, other metals such as stainless steel, gold and silver, have also been used as HER electrode substrates [66–68]. Considering the inert property of silver and gold, active catalysts are generally deposited onto the substrate surfaces. For example, Uosaki et al. [68] prepared an HER electrode by depositing boron nitride nanosheets on a gold substrate, and the electrode exhibited an overpotential only −30 mV greater than Pt/C to reach the current density of 5 mA cm^{-2} in 0.5 M H_2SO_4. Kiani et al. [69] fabricated a platinum-coated nanoporous gold film as HER electrode, which delivered a current density of 198 mA cm^{-2} at −0.8 V vs. Ag/AgCl and a mass activity of 1940 mA μg^{-1}. However, the high costs and low reserves of precious metals (silver, gold and platinum) have severely limited their practical applications. Several studies have shown that earth-abundant, low-cost metal substrates can be used for the preparation of HER electrodes, such as stainless steel mesh, stainless steel rod, molybdenum mesh [65–67]. For example, Xu et al. synthesized three-dimensional (3D) arrays of MoS_2 nanosheets on a Mo mesh as an HER electrode by hydrothermal treatment in an aqueous thiourea solution, which exhibited an η_{10} of −160 mV in acid (Fig. 5) [65]. In spite of a low cost and apparent HER performance, the properties such as corrosion resistance and HER kinetics have rarely been studied, and their feasibility and sustainability in HER remain to be explored.

3. Porous carbon-based electrodes

3.1. Carbon cloth/paper/felt-based electrodes

Compared to metal-based electrodes, carbon materials have the unique advantages of low cost, high specific surface area, abundant pore structure, tunable elemental doping, and good chemical stability, making them promising electrode supports. In fact, the HER performance of carbon-based electrodes can be effectively improved through deliberate structural engineering.

Among the different carbon substrates, carbon cloth, carbon paper and carbon felt are the most commonly used electrode supports with

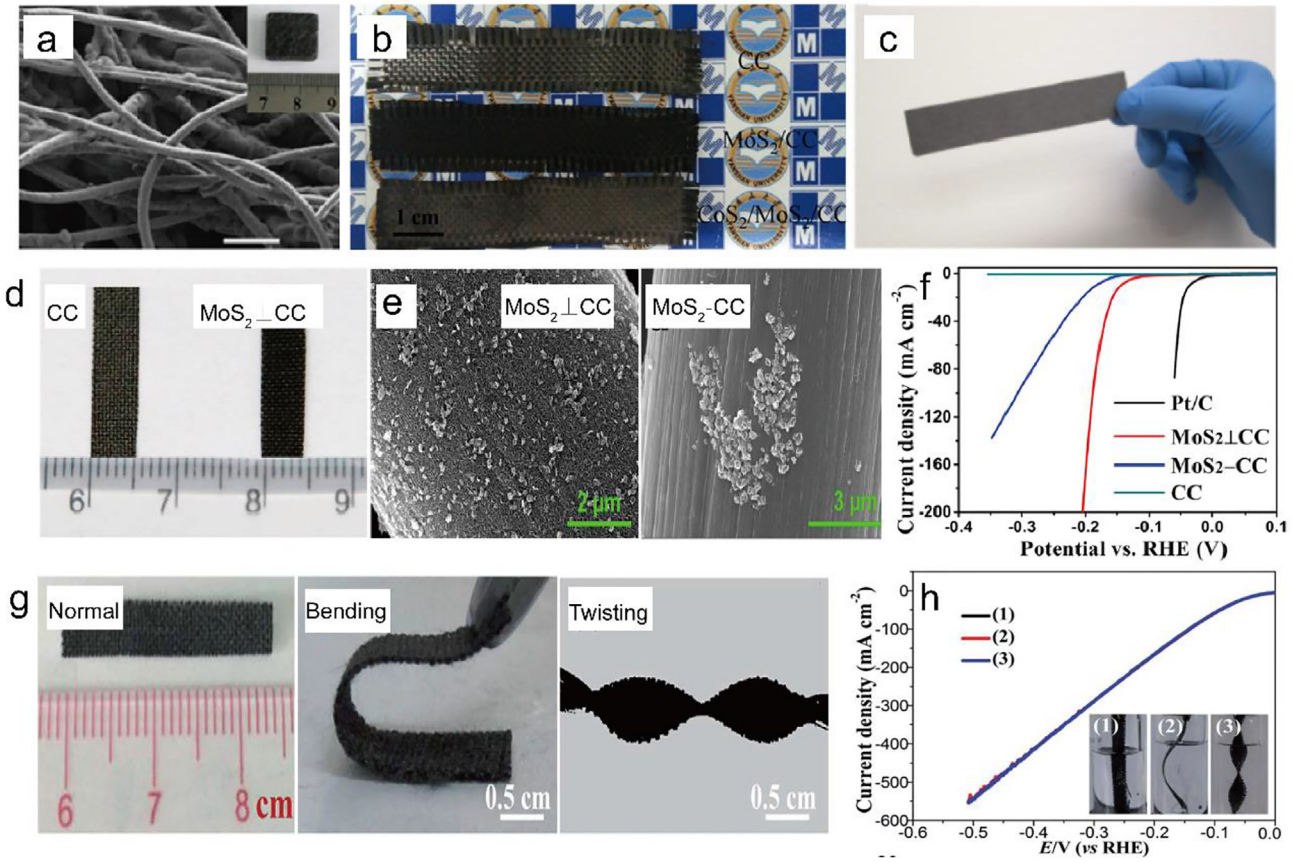

Fig. 6. (a) SEM of carbon felt. Inset is a corresponding photograph. Panel (a) reproduced with permission from Ref. [70] © American Chemical Society. (b) Photograph of carbon cloth. Panel (b) reproduced with permission from Ref. [71] © Elsevier. (c) Photograph of carbon paper. Panel (c) reproduced with permission from Ref. [72] © American Chemical Society. (d) photograph of blank CC and MoS_2⊥CC, (e) SEM images of MoS_2⊥CC and MoS_2-CC, and (f) HER polarization curves of varied electrodes. Panels (d-f) reproduced with permission from Ref. [73] © American Chemical Society, (g) Photographs and (h) polarization curves of carbon cloth under the various distorted states. Panels (g, h) reproduced with permission from Ref. [74] © Royal Society of Chemistry.

high electrical conductivity, interconnected pores and chemical stability. These features endow the HER electrode with high durability, facile ion diffusion and increased catalytic activity (Fig. 6a–c). In the traditional electrode fabrication, the nanocatalyst power is dispersed into a solution with the addition of a binder to prepare the catalyst ink, which is then coated onto the carbon substrates. For example, Chanda et al. [75] prepared an HER electrode by coating $NiFe_2O_4$ catalysts onto a carbon substrate using poly(phenylene oxide) ionomer, polytetrafluoroethylene and Nafion®, and observed that the HER electrode with the poly(phenylene oxide) ionomer achieved the best performance. However, the use of an electrical insulating binder may decrease electrical conductivity of the electrode, block catalytic active sites and hinder ion diffusion within electrodes, hence resulting in a reduced electrocatalytic performance.

In addition, aggregation and peeling off of catalysts from substrates may occur [76]. Recently, many studies have shown that binder-free HER electrodes can be prepared by direct growth of catalysts on the carbon cloth/carbon paper/felt substrates using hydrothermal, solvothermal or electrochemical methods. For example, Zhang et al. [73] prepared a binder-free electrode by growing MoS_2 nanosheets vertically on carbon cloth (MoS_2⊥CC), and a binder-based electrode by physically coating MoS_2 on carbon cloth using Nafion (MoS_2-CC) (Fig. 6d–e), and found that MoS_2⊥CC delivered a current density of 200 mA cm^{-2} at the overpotential of −205 mV in acidic media, whereas it was only ca. 20 mA cm^{-2} for MoS_2-CC (Fig. 6f). This can be attributed to the well-dispersed MoS_2 on the porous skeleton that facilitated ion diffusion in the binder-free electrode [77]. In another study, Wang et al. [74] reported a new type of Ni_2P–CoP hybrid nanosheet array on carbon cloth (Ni_2P–CoP HNSAs/CC), which exhibited a high HER performance with a small η_{10} of −85 mV and high stability with only a 12.49% loss of current density after 14 h's discharging at a constant potential of −0.14 V vs. RHE. Importantly, the as-developed cathode also showed an excellent flexibility and virtually no change of the HER performance under various bending and twisting states. These results confirmed the feasibility and reliability of this electrode in practical applications (Fig. 6g and h).

It should be noted that although many studies have demonstrated satisfactory performance of binder-free electrodes in all-pH media, the HER catalysts are usually adhered on the surfaces of porous carbon or carbon felt substrate, and the interconnected pore structures are not sufficiently utilized. This may compromise the eventual performance.

3.2. Graphene/Carbon nanotube film-based electrodes

Considering the low utilization rate of porous carbon cloth/paper/felt, the electrodes can be constructed by mixing HER catalysts, such as WS_2, and Co nanoparticles, with graphene or carbon nanotubes, and then filtering the mixture to obtain a thin film in which the catalysts are homogenously dispersed [76,78]. For example, Hou et al. [78] prepared a Co nanoparticles@nitrogen-doped graphene film (Co@NGF) as a flexible, porous electrode. The procedure involves three steps: (a) mixing a graphene oxide suspension with a dicyandiamide–cobalt complex to form a homogenous mixture; (b) filtration of the mixture to obtain a nanostructured film; and (c) annealing of the prepared film at 700 °C in an Ar atmosphere to obtain Co@NGF. The resulting film electrode achieved an E_{onset} of −14 mV and η_{10} of −124.6 mV in acidic

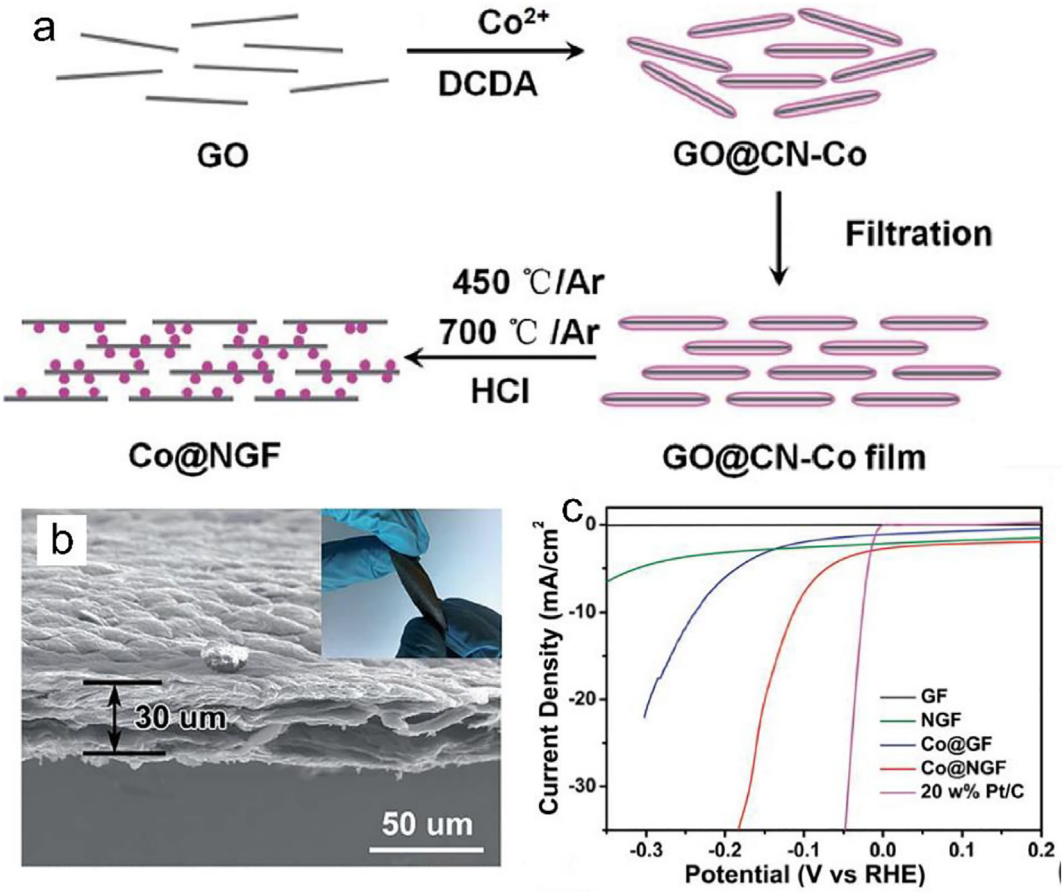

Fig. 7. (a) Schematic illustration of the synthesis and (b) SEM image of Co@NGF, (c) HER polarization curves of varied electrodes. Inset to (b) is a photograph of the Co@NGF electrode. Reproduced with permission from Ref. [78] © Royal Society of Chemistry.

media (Fig. 7). Apparently, the catalyst electrodes based on graphene and carbon nanotube have a sufficient catalyst/electrode contact area and high catalyst utilization rate due to the homogeneously dispersed catalysts. In addition, in combination with the high specific surface area and high porosity, the catalyst electrode can obtain an extended exposure of active sites and facilitated ion diffusion within the electrode.

3.3. Graphene/carbon nanotube/carbon fiber aerogel-based electrodes

3D carbon materials such as graphene aerogel, carbon nanotube aerogel and carbon fiber aerogel can provide a high specific surface area (and electroactive surface area), abundant 3D interconnected network, enhanced accessibility by electrolytes, and multidimensional electron/ion transport channels (Fig. 8a), as compared to carbon cloth/carbon paper and graphene/carbon nanotube films [79,81]. These features make them promising supports in HER electrode fabrication. Typically, HER electrodes based on graphene aerogels are prepared in two steps: (1) self-assembly of graphene/carbon nanotube/carbon fiber hydrogel/aerogel by direct pyrolysis or hydrothermal method, and (2) decoration of catalysts on the obtained carbon support. For example, Zhao et al. [79] prepared 3D graphene aerogel-supported MoS_2 nanosheets (GA-MoS_2) as an HER electrode by (a) hydrothermal self-assembly to form a graphene hydrogel, (b) a second hydrothermal treatment of the hydrogel in an aqueous solution containing ammonium heptamolybdate and thiourea to grow the MoS_2 nanosheets onto the hydrogel surface, and (c) freeze-drying to obtain the final product (Fig. 8b). To simplify the preparation procedure, Zhang et al. [21] fabricated a cobalt phosphide nanoparticles-decorated 3D graphene aerogel electrode. Experimentally, graphene oxide and Co^{2+} were self-assembled to form a graphene hydrogel, which was then freeze-dried and thermally treated and phosphidated to obtain cobalt phosphide nanoparticles-decorated 3D graphene aerogel (Fig. 8c). Zhang et al. [80] synthesized a cotton wool-derived carbon fiber aerogel as an electrode support by direct carbonization, instead of hydrothermal, solvothermal and freezing dry, significantly simplifying the preparation procedure of aerogels (Fig. 8d). Considering the high exposure of active sites, and multidimensional transport channels for electron and ions, these aerogel electrodes exhibited an improved HER performance. For example, Xu et al. [82] synthesized penroseite (Ni, Co)Se_2 nanocages anchored on a 3D graphene aerogel as HER electrodes, which exhibited an η_{10} of −156 mV in 1 M KOH, only 28 mV higher than that of Pt/C. Nevertheless, the pore structures of aerogel electrodes may collapse during actual, long-term operation, especially for the electrodes prepared by hydrothermal and freeze drying processes, due to the limited π–π interaction between carbon precursors.

3.4. Carbon foam-based electrodes

Different from the procedure for the preparation of graphene/carbon nanotube aerogels, one commonly used method to prepare carbon foam is direct pyrolysis of porous precursors, such as citric acid monohydrate, melamine, glucose and polyimide [83–86]. During the pyrolysis process, the precursors are dehydrated and polymerized, and the rapid release of H_2O molecules leads to the formation of 3D carbon foam networks [84]. For instance, Park et al. [83] fabricated carbon foam/N-doped graphene@MoS_2 hybrid nanostructures as HER electrodes by using melamine sponge as the raw material to prepare carbon foam and N-doped graphene@MoS_2 as the active component (Fig. 9a), and the as-prepared electrode achieved a low η_{10} of −170 mV in 0.5 M H_2SO_4. Another unique advantage of carbon foam is that heteroatom

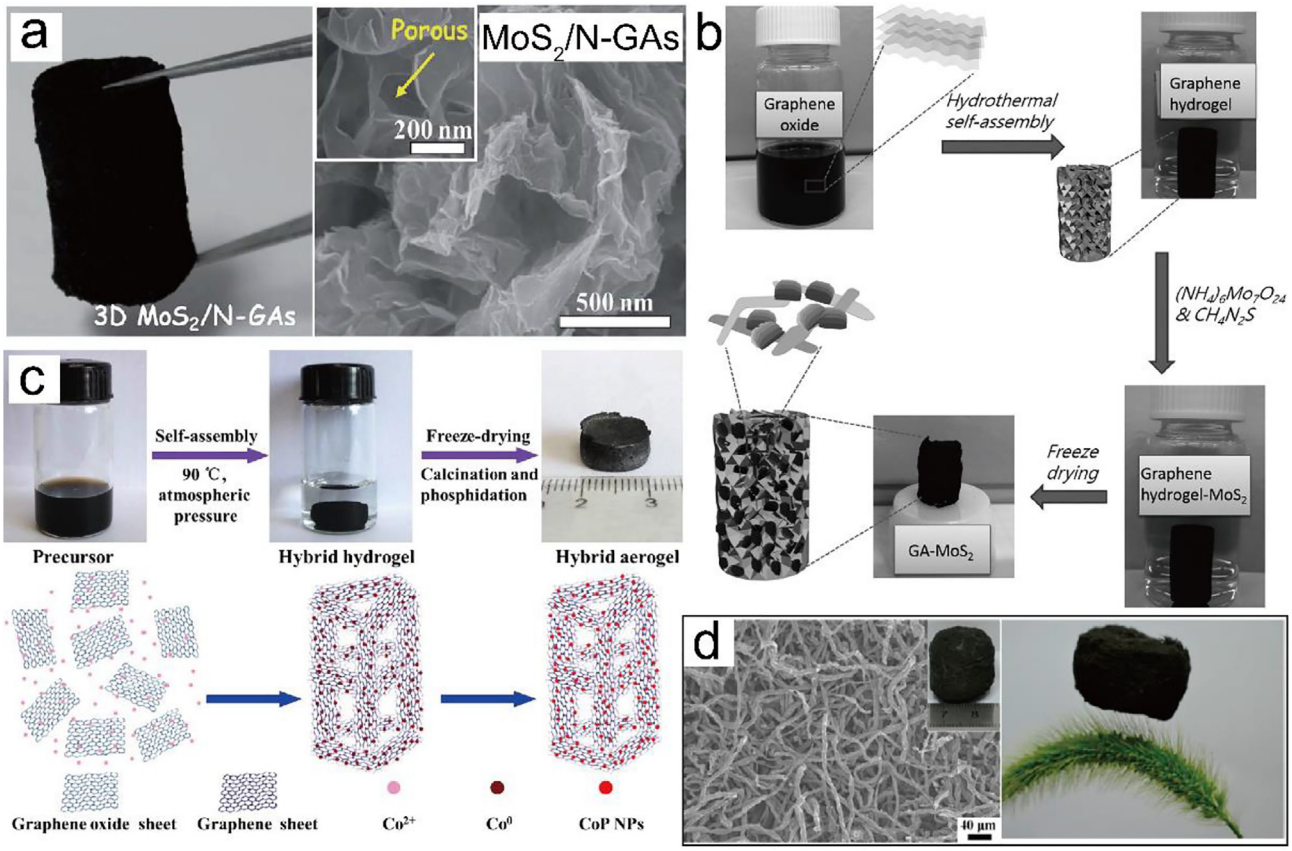

Fig. 8. (a) Photograph (left) and SEM (right) images of graphene aerogel decorated with MoS_2. Panel (a) reproduced with permission from Ref. [30] © Royal Society of Chemistry. (b) Preparation procedure of GA-MoS_2 composite. Panel (b) reproduced with permission from Ref. [79] © Wiley. (c) Fabrication process for the graphene aerogel electrode decorated with cobalt phosphide nanoparticles. Panel (c) reproduced with permission from Ref. [21] © Wiley. (d) SEM image and photograph of carbon fiber aerogel. Panel (d) reproduced with permission from Ref. [80] © American Chemical Society.

doping can be concurrently achieved with the formation of a 3D foam network during pyrolysis. For example, Wang et al. [84] prepared a Ni_3C nanoparticles-embedded carbon foam electrode (Ni_3C@PCN) by carbonizing the mixture of citric acid monohydrate and nickel acetate tetrahydrate, leading to the formation of a foam network and the incorporation of Ni_3C nanoparticle. Significantly, the as-prepared Ni_3C@PCN electrode exhibited an E_{onset} of −65 mV and η_{20} of −203 mV in acidic media (Fig. 9b–e), and also showed only a negligible loss of the current density during 1000 cycles.

The carbon foam electrode prepared by pyrolysis is usually much more stable than that formed through π–π interaction between carbon precursors, providing a stronger mechanical performance. Unlike a multistep synthesis process, direct pyrolysis does not require rigorous conditions or high-cost templates. However, one challenge remains: the formation of a porous structure in carbon foam mainly relies on the raw material and the pyrolysis process; and the lack of control in pyrolysis can result in a low degree of porosity and hence hinder the penetration of electrolyte in the interior space of carbon foam electrode.

4. Other emerging electrodes

As discussed above, porous electrodes with a large surface area, abundant mesoporosity/macroporosity and a conductive skeleton can provide multiple pathways to facilitate fast ion diffusion and electron transfer. However, the low availability and controllability of pore structure in the electrode are two crucial limitations which can not be resolved yet by chemical methods, such as pyrolysis, hydrothermal treatment, and templates. Interestingly, 3D printing technology has emerged as an effective fabrication tool for rapid prototyping and can achieve a rational electrode design for an accurate control of electrode porosity. This can effectively increase the formation of pores inside the electrode and facilitate ion and bubble transport. Generally, computer numerical control additive manufacturing of 3D printing can take advantage of various precursor materials, such as polymer, graphene oxide and stainless steel, allowing for the fabrication of products with different physical, chemical, mechanical, and electrical properties [87–89]. For example, Ambrosi et al. [90] prepared stainless-steel electrodes using selective laser melting additive manufacturing and then electrochemically modified the electrode surface to alter the surface composition and tune its catalytic properties by depositing Pt as the HER catalyst and IrO_2 as the oxygen evolution reaction (OER) catalyst. Experimentally, the as-prepared electrode was then used in an electrolyzer in 1 M KOH, which achieved efficient hydrogen and oxygen evolution with a small voltage of 1.5 V (Fig. 10). This study strongly demonstrated the feasibility of building electrodes and electrochemical cells via 3D metal and polymer printing [90]. Nevertheless, despite many advantages, 3D printed electrodes based on carbon materials have not been reported so far. Further research is strongly desired.

Furthermore, current studies mainly focus on the improvement of the electroactive surface area, electron transfer and ion diffusion in the HER electrode through the optimization of pore structure, heteroatom doping and nanoparticles incorporation [83,91–95]. However, as HER is an electrochemical process involving also ion diffusion and bubble formation, transport and release, the eventual HER performance is actually determined by these factors combined. Improved ion diffusion and electron transfer will effectively facilitate the hydrogen evolution rate and the formation of hydrogen bubbles on the electrode surface. However, the massive bubbles adhered on the surface of electrode will decrease the effective surface area and hinder the electron-transfer reaction and ion diffusion, thus conversely deteriorating the HER

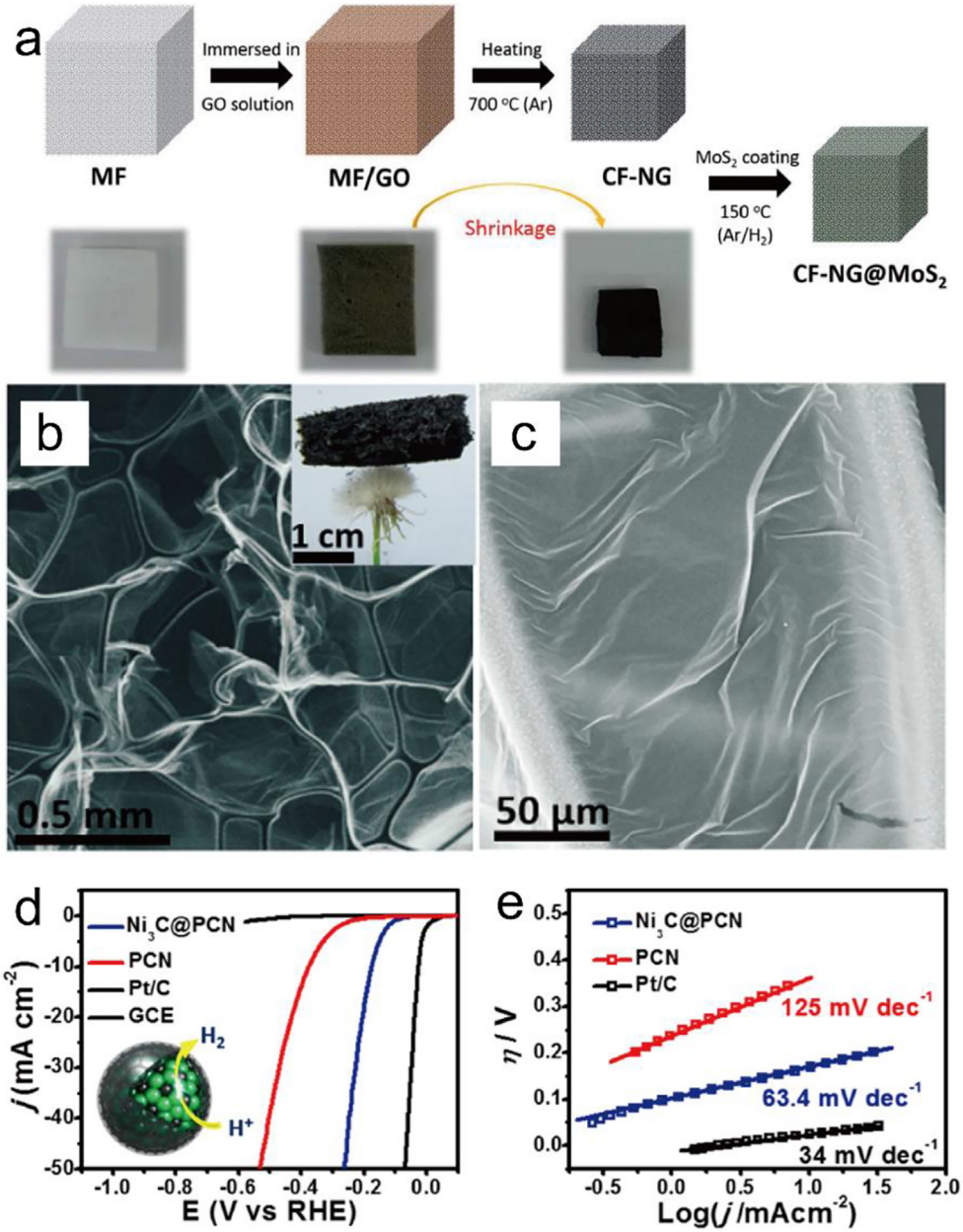

Fig. 9. (a) Preparation procedure for carbon foam/N-doped graphene@MoS_2 hybrid. Panel (a) reproduced with permission from Ref. [83] © Royal Society of Chemistry. (b, c) SEM images of Ni_3C@PCN (inset to panel b is a photograph of the sample), (d) polarization and (e) Tafel curves of varied electrodes. Panels (b-e) reproduced with permission from Ref. [84] © American Chemical Society.

performance. Therefore, the release of hydrogen bubbles from the electrode surface is a key point to improve both effective electroactive surface area and electron transfer and ion diffusion. The bubbles on the electrode surface experience three forces: buoyance force which is proportional to the bubble volume, gravity which is proportional to the mass of the hydrogen bubbles, and adhesion force from the underlying catalyst film. Among these, gravity is negligible duo to the much lower density of hydrogen bubbles compared to the electrolyte. It is generally accepted that the detachment of bubbles requires a buoyance force higher than adhesion forces. Therefore, a higher adhesion force would cause a larger detachment diameter and adhesion surface area of bubbles on the electrode. "Superaerophobic" surfaces have been reported as an effective structure to decrease the adhesion force and to diminish the negative effects caused by the adhered hydrogen bubbles. It has been reported that the adhesion force originates from solid–liquid–gas TPCL, and nanostructured surface can create a discontinuous TPCL and hence decrease the adhesion force of bubbles on the electrode surface, leading to a small release size and fast removal of hydrogen bubbles at high reaction rates (Fig. 11a–c). For example, Lu et al. [28] constructed a MoS_2 nanostructured HER electrode with a gas bubble contact angle of 153.6 ± 2.4°, which is higher than 135.2 ± 3.3° for a flat MoS_2 film electrode. Adhesive force measurements with 3 μL bubbles revealed that the as-prepared electrode exhibited a low adhesive force of 10.8 ± 1.7 μN, as compared to 124.8 ± 6.1 μN for flat MoS_2 film. Eventually, H_2 bubbles on the MoS_2 nanostructured electrode were detached with an average diameter less than 100 μm (> 500 μm for flat MoS_2 film) (Fig. 11d and e). Therefore, surface nanoengineering is an effective approach to reduce the solid–gas interaction in electrode fabrication, and to facilitate the release of hydrogen bubbles and ion diffusion. Indeed, nanostructures, such as nanowires, nanorods, nanoflakes, nanosheets, nanoflowers and nanotube arrays, have been widely used for the fabrication of superaerophobic

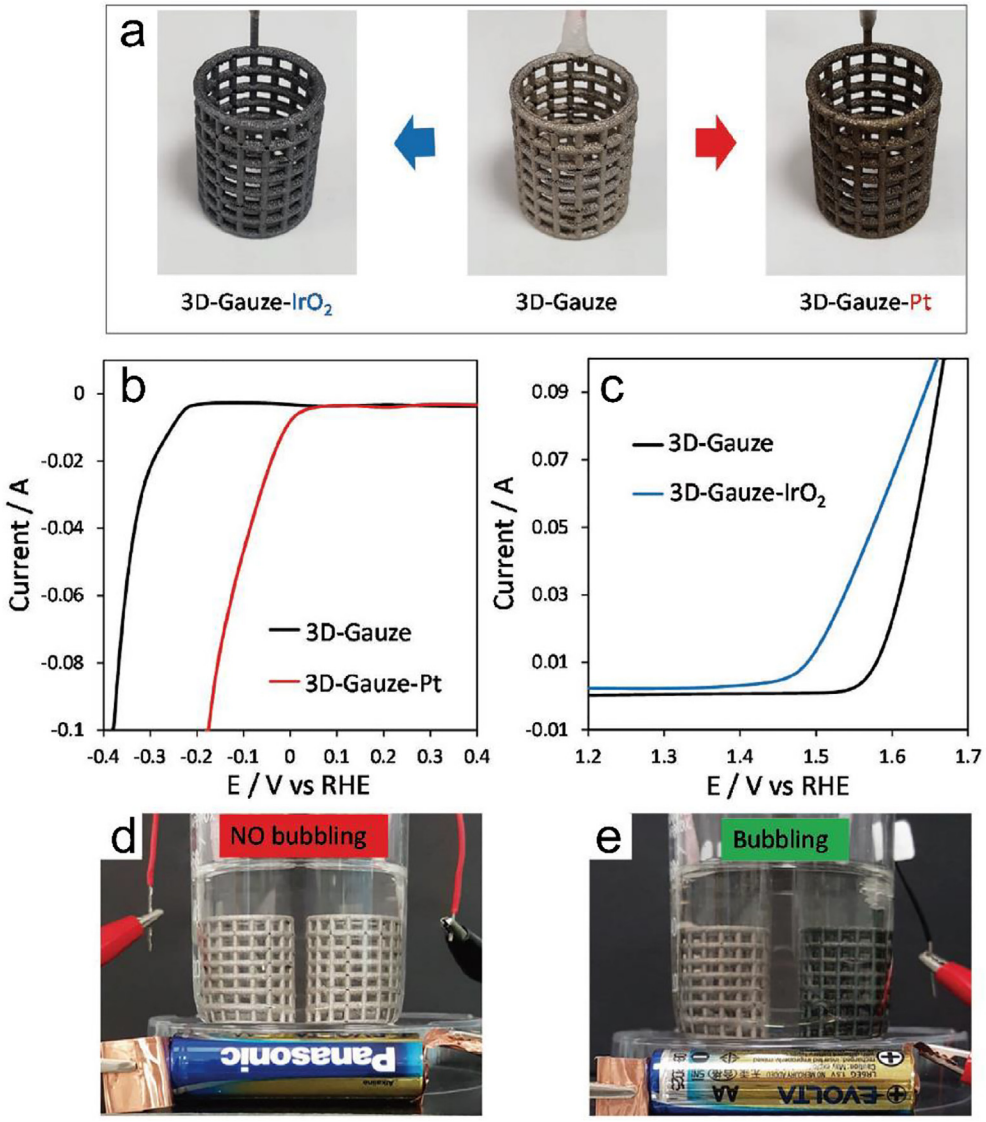

Fig. 10. (a) Photographs of 3D-printed gauze steel electrodes with electrochemical surface modification, (b) HER and (c) OER polarization curves in 1 M KOH, video snapshots of water splitting operations in 1 M KOH using (d) bare 3D-gauze electrodes as the anode and cathode and (e) Pt-modified 3D-gauze as the cathode and IrO_2-modified 3D-gauze as the anode. Reproduced with permission from Ref. [90] © Wiley.

HER electrodes [28,29,96–98]. The mechanism of superaerophobic surface construction can also be expanded to other gas evolution reactions, such as oxygen evolution, and chlorine evolution [99,100].

Apart from the release of hydrogen bubbles from electrode surface, the transport of bubbles in the porous structure of electrode has received negligible attention thus far. Actually, as the charge transfer kinetics on the catalyst surface have been substantially improved, the HER overpotential may be dominated by mass transport, especially at a high current density. The transport of bubbles inside the porous structure of the electrode, such as nickel/copper foam, not only affects the effective surface area in the interior of electrode, but also influences the penetration of electrolyte. Reasonably, it can be understood that the bubbles may be adhered or plugged in the pores of electrode when the bubble size is larger than the pore size. In contrast, the bubbles are likely to diffuse out of the electrode when the bubble size is smaller than the pore size of the electrode. For example, Xu et al. [32] synthesized nanostructured NiMo alloy on metal foam as a superaerophobic electrode, and observed that the hydrogen bubbles were generated and left quickly with a small average releasing diameter of ca. 32 μm. However, in the control electrode, the as-produced H_2 bubbles grew gradually in size and plugged severely within the skeleton of the metal foam electrode. In fact, the as-obtained electrode delivered an excellent performance that was about three times better than those of commercial Pt/C and IrO_2/C catalysts-based electrodes at 1.9 V. Therefore, the pore size and bubble release diameter can be critical factors determining the bubble removal in the interior of the electrode. Inevitably, superaerophobic pores will decrease the release size and facilitate the removal of bubbles from the pores. Thus, rational design of the pore structure is a feasible method to prevent the blocking of bubbles in the electrodes in the practical applications.

5. Conclusions and perspectives

In this review, we analyze the correlation between electron transfer, ion diffusion, bubble release within the electrode and the corresponding electrochemical HER performance. With an apparent intrinsic activity of the catalysts, ion diffusion and bubble release stand out as two critical factors that may dictate the eventual HER performance. Thus, in this review we summarize recent progress in the development of effective strategies for the design and fabrication of HER electrodes, and compare the HER performance in these fabrication methods within the context of ion diffusion, bubble release, and HER performance. Such

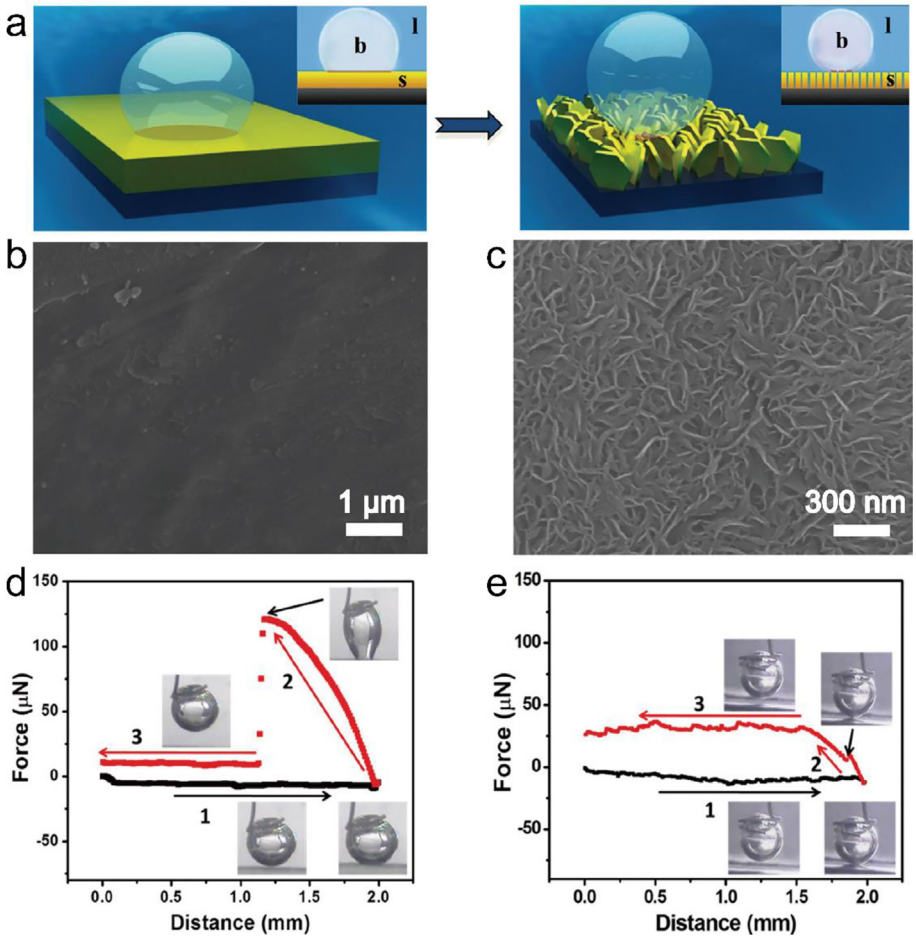

Fig. 11. (a) Schematic illustration of adhesion behaviors of gas bubbles on flat film (left) and nanostructured film (right). Insets are the side views to show the different intact and discontinuous TPCL on flat and nanostructured films, and the different contact angles. (b) and (c) SEM images of flat and nanostructured MoS_2, (d) and (e) adhesive forces measurements of the gas bubbles on flat and nanostructured MoS_2 films. Reproduced with permission from Ref. [28] © Wiley.

fundamental insights are critical in the utilization of the catalysts for the construction of high-performance HER electrodes.

Nevertheless, despite apparent progress, challenging issues remain. For instance, in practical applications, the consumption of protons will not only lead to alkalization of the electrolyte on the cathode surface but also pH polarization between the anode and cathode. This necessitates the development of high-efficiency HER electrodes in a wide pH range that can overcome the increasing concentration overpotential. In addition, further research is needed to advance the technology of 3D printing for the preparation of carbonaceous HER electrodes so as to take advantage of the extensive progress of carbon-based HER catalysts. Furthermore, the durability and sustainability of superaerophobic surfaces is another critical issue of HER electrodes, because vibration, stress and electrolyte flow may destroy the electrode structure during long-term operation. Further breakthroughs are urgently needed in the design, construction and nanoengineering of the electrodes.

Author contributions

The manuscript was written through contributions of all authors. All authors have given approval to the final version of the manuscript.

Declaration of Competing Interest

The authors declare that they have no known competing financial interests or personal relationships that could have appeared to influence the work reported in this paper.

Acknowledgements

This work was supported by the National Natural Science Foundation for Young Scientists of China (51906168 and 51606172) and the US National Science Foundation (CBET-1848841 and CHE-1900235).

References

[1] W.J. Zhou, J. Jia, J. Lu, L.J. Yang, D.M. Hou, G.Q. Li, S.W. Chen, Recent developments of carbon-based electrocatalysts for hydrogen evolution reaction, Nano Energy 28 (2016) 29–43.
[2] Y. Liang, Y. Li, H. Wang, H. Dai, Strongly coupled inorganic/nanocarbon hybrid materials for advanced electrocatalysis, J. Am. Chem. Soc. 135 (2013) 2013–2036.
[3] M. Gong, D.Y. Wang, C.C. Chen, B.J. Hwang, H.J. Dai, A mini review on nickel-based electrocatalysts for alkaline hydrogen evolution reaction, Nano Res. 9 (2016) 28–46.
[4] B. Song, S. Jin, Two are better than one: heterostructures improve hydrogen evolution catalysis, Joule 1 (2017) 220–221.
[5] X.P. Ren, Q. Ma, H.B. Fan, L.Q. Pang, Y.X. Zhang, Y. Yao, X.D. Ren, S.Z. Liu, A Se-doped MoS_2 nanosheet for improved hydrogen evolution reaction, Chem. Commun. 51 (2015) 15997–16000.
[6] C.Q. Sun, J.Y. Zhang, J. Ma, P.T. Liu, D.Q. Gao, K. Tao, D.S. Xue, N-doped WS_2 nanosheets: a high-performance electrocatalyst for the hydrogen evolution reaction, J. Mater. Chem. A 4 (2016) 11234–11238.
[7] S.S. Yang, M. Xie, L.L. Chen, W. Wei, X.M. Lv, Y.G. Xu, N. Ullah, O.C. Judith, Y.B. Adegbemiga, J.M. Xie, Cobalt phosphide nanoparticles embedded in 3D N-doped porous carbon for efficient hydrogen and oxygen evolution reactions, Int. J. Hydrogen Energy 44 (2019) 4543–4552.
[8] Q. Tang, D.E. Jiang, Mechanism of Hydrogen Evolution Reaction on 1T-MoS_2 from First Principles, ACS Catal. 6 (2016) 4953–4961.
[9] N.C. Cheng, S. Stambula, D. Wang, M.N. Banis, J. Liu, A. Riese, B.W. Xiao, R.Y. Li, T.K. Sham, L.M. Liu, G.A. Botton, X.L. Sun, Platinum single-atom and cluster

catalysis of the hydrogen evolution reaction, Nat. Commun. 7 (2016) 13638.
[10] G.L. Ye, Y.J. Gong, J.H. Lin, B. Li, Y.M. He, S.T. Pantelides, W. Zhou, R. Vajtai, P.M. Ajayan, Defects engineered monolayer MoS_2 for improved hydrogen evolution reaction, Nano Lett. 16 (2016) 1097–1103.
[11] J. Mahmood, F. Li, S.M. Jung, M.S. Okyay, I. Ahmad, S.J. Kim, N. Park, H.Y. Jeong, J.B. Baek, An efficient and pH-universal ruthenium-based catalyst for the hydrogen evolution reaction, Nat. Nanotechnol. 12 (2017) 441–446.
[12] J. Kibsgaard, C. Tsai, K. Chan, J.D. Benck, J.K. Norskov, F. Abild-Pedersen, T.F. Jaramillo, Designing an improved transition metal phosphide catalyst for hydrogen evolution using experimental and theoretical trends, Energy Environ. Sci. 8 (2015) 3022–3029.
[13] W. Liu, E.Y. Hu, H. Jiang, Y.J. Xiang, Z. Weng, M. Li, Q. Fan, X.Q. Yu, E.I. Altman, H.L. Wang, A highly active and stable hydrogen evolution catalyst based on pyrite-structured cobalt phosphosulfide, Nat. Commun. 7 (2016) 10771.
[14] H.Y. Jin, J. Wang, D.F. Su, Z.Z. Wei, Z.F. Pang, Y. Wang, In situ cobalt-cobalt oxide/N-doped carbon hybrids As superior bifunctional electrocatalysts for hydrogen and oxygen evolution, J. Am. Chem. Soc. 137 (2015) 2688–2694.
[15] L. Ma, L.R.L. Ting, V. Molinari, C. Giordano, B.S. Yeo, Efficient hydrogen evolution reaction catalyzed by molybdenum carbide and molybdenum nitride nanocatalysts synthesized via the urea glass route, J. Mater. Chem. A 3 (2015) 8361–8368.
[16] P. Xiao, X.M. Ge, H.B. Wang, Z.L. Liu, A. Fisher, X. Wang, Novel molybdenum carbide-tungsten carbide composite nanowires and their electrochemical activation for efficient and stable hydrogen evolution, Adv. Funct. Mater. 25 (2015) 1520–1526.
[17] N. Ullah, W. Zhao, X. Lu, C.J. Oluigbo, S.A. Shah, M. Zhang, J. Xie, Y. Xu, In situ growth of M-MO (M= Ni, Co) in 3D graphene as a competent bifunctional electrocatalyst for OER and HER, Electrochim. Acta 298 (2019) 163–171.
[18] J.Q. Tian, Q. Liu, A.M. Asiri, X.P. Sun, Self-supported nanoporous cobalt phosphide nanowire arrays: an efficient 3D hydrogen-evolving cathode over the wide range of pH 0–14, J. Am. Chem. Soc. 136 (2014) 7587–7590.
[19] Y.H. Liang, Q. Liu, A.M. Asiri, X.P. Sun, Y.L. Luo, Self-supported FeP nanorod arrays: a cost-effective 3D hydrogen evolution cathode with high catalytic activity, ACS Catal. 4 (2014) 4065–4069.
[20] P. Jiang, Q. Liu, Y.H. Liang, J.Q. Tian, A.M. Asiri, X.P. Sun, A cost-effective 3D hydrogen evolution cathode with high catalytic activity: FeP nanowire array as the active phase, Angew. Chem. Int. Ed. 53 (2014) 12855–12859.
[21] X.P. Zhang, Y.J. Han, L. Huang, S.J. Dong, 3D graphene aerogels decorated with cobalt phosphide nanoparticles as electrocatalysts for the hydrogen evolution reaction, ChemSusChem 9 (2016) 3049–3053.
[22] A. Sivanantham, P. Ganesan, S. Shanmugam, Hierarchical $NiCo_2S_4$ nanowire arrays supported on Ni foam: an efficient and durable bifunctional electrocatalyst for oxygen and hydrogen evolution reactions, Adv. Funct. Mater. 26 (2016) 4661–4672.
[23] Z.Y. Zhang, W.Y. Li, M.F. Yuen, T.W. Ng, Y.B. Tang, C.S. Lee, X.F. Chen, W.J. Zhang, Hierarchical composite structure of few-layers MoS_2 nanosheets supported by vertical graphene on carbon cloth for high-performance hydrogen evolution reaction, Nano Energy 18 (2015) 196–204.
[24] A. Behranginia, M. Asadi, C. Liu, P. Yasaei, B. Kumar, P. Phillips, T. Foroozan, J.C. Waranius, K. Kim, J. Abiade, R.F. Klie, L.A. Curtiss, A. Salehi-Khojin, Highly efficient hydrogen evolution reaction using crystalline layered three-dimensional molybdenum disulfides grown on graphene film, Chem. Mater. 28 (2016) 549–555.
[25] R. Zhang, X.X. Wang, S.J. Yu, T. Wen, X.W. Zhu, F.X. Yang, X.N. Sun, X.K. Wang, W.P. Hu, Ternary $NiCo_2Px$ nanowires as ph-universal electrocatalysts for highly efficient hydrogen evolution reaction, Adv. Mater. 29 (2017) 1605502.
[26] P. Shanmugam, A.P. Murthy, J. Theerthagiri, W. Wei, J. Madhavan, H.S. Kim, T. Maiyalagan, J.X. Xie, Robust bifunctional catalytic activities of N-doped carbon aerogel-nickel composites for electrocatalytic hydrogen evolution and hydrogenation of nitrocompounds, Int. J. Hydrogen Energy 44 (2019) 13334–13344.
[27] Y.Q. Shi, W. Gao, H.Y. Lu, Y.P. Huang, L.Z. Zuo, W. Fan, T.X. Liu, Carbon-nanotube-incorporated graphene scroll-sheet conjoined aerogels for efficient hydrogen evolution reaction, ACS Sustain. Chem. Eng. 5 (2017) 6994–7002.
[28] Z.Y. Lu, W. Zhu, X.Y. Yu, H.C. Zhang, Y.J. Li, X.M. Sun, X.W. Wang, H. Wang, J.M. Wang, J. Luo, X.D. Lei, L. Jiang, Ultrahigh hydrogen evolution performance of under-water "superaerophobic" MoS_2 nanostructured electrodes, Adv. Mater. 26 (2014) 2683–2687.
[29] Y.J. Li, H.C. Zhang, T.H. Xu, Z.Y. Lu, X.C. Wu, P.B. Wan, X.M. Sun, L. Jiang, Under-Water Superaerophobic Pine-Shaped Pt Nanoarray Electrode for Ultrahigh-Performance Hydrogen Evolution, Adv. Funct. Mater. 25 (2015) 1737–1744.
[30] Y. Hou, B. Zhang, Z.H. Wen, S.M. Cui, X.R. Guo, Z. He, J.H. Chen, A 3D hybrid of layered MoS_2/nitrogen-doped graphene nanosheet aerogels: an effective catalyst for hydrogen evolution in microbial electrolysis cells, J. Mater. Chem. A 2 (2014) 13795–13800.
[31] R.T. Perera, C.E. Arcadia, J.K. Rosenstein, Probing the nucleation, growth, and evolution of hydrogen nanobubbles at single catalytic sites, Electrochim. Acta 283 (2018) 1773–1778.
[32] W.W. Xu, Z.Y. Lu, P.B. Wan, Y. Kuang, X.M. Sun, High-performance water electrolysis system with double nanostructured superaerophobic electrodes, Small 12 (2016) 2492–2498.
[33] J.E. George, S. Chidangil, S.D. George, Recent progress in fabricating superaerophobic and superaerophilic surfaces, Adv. Mater. Interfaces 4 (2017) 1601088.
[34] A.R. Zeradjanin, J.P. Grote, G. Polymeros, K.J.J. Mayrhofer, A critical review on hydrogen evolution electrocatalysis: re-exploring the volcano-relationship, Electroanalysis 28 (2016) 2256–2269.
[35] C.G. Morales-Guio, L.A. Stern, X.L. Hu, Nanostructured hydrotreating catalysts for electrochemical hydrogen evolution, Chem. Soc. Rev. 43 (2014) 6555–6569.
[36] H.T. Du, R.M. Kong, X.X. Guo, F.L. Qu, J.H. Li, Recent progress in transition metal phosphides with enhanced electrocatalysis for hydrogen evolution, Nanoscale 10 (2018) 21617–21624.
[37] B.J. Zhu, R.Q. Zou, Q. Xu, Metal-organic framework based catalysts for hydrogen evolution, Adv. Energy Mater. 8 (2018) 1801193.
[38] L.Z. Zhang, Y. Jia, X.C. Yan, X.D. Yao, Activity origins in nanocarbons for the electrocatalytic hydrogen evolution reaction, Small 14 (2018) 1800235.
[39] Z.H. Pu, C. Tang, Y.L. Luo, Ferric phosphide nanoparticles film supported on titanium plate: a high-performance hydrogen evolution cathode in both acidic and neutral solutions, Int. J. Hydrogen Energy 40 (2015) 5092–5098.
[40] W.J. Zhou, Y.C. Zhou, L.J. Yang, J.L. Huang, Y.T. Ke, K. Zhou, L.G. Li, S.W. Chen, N-doped carbon-coated cobalt nanorod arrays supported on a titanium mesh as highly active electrocatalysts for the hydrogen evolution reaction, J. Mater. Chem. A 3 (2015) 1915–1919.
[41] M.A. Amin, S.A. Fadlallah, G.S. Alosaimi, In situ aqueous synthesis of silver nanoparticles supported on titanium as active electrocatalyst for the hydrogen evolution reaction, Int. J. Hydrogen Energy 39 (2014) 19519–19540.
[42] Z.H. Pu, Q. Liu, P. Jiang, A.M. Asiri, A.Y. Obaid, X.P. Sun, CoP nanosheet arrays SUPPORTED ON a Ti plate: an efficient cathode for electrochemical hydrogen evolution, Chem. Mater. 26 (2014) 4326–4329.
[43] H.Q. Xiao, S.T. Wang, C. Wang, Y.Y. Li, H.R. Zhang, Z.J. Wang, Y. Zhou, C.H. An, J. Zhang, Lamellar structured $CoSe_2$ nanosheets directly arrayed on Ti plate as an efficient electrochemical catalyst for hydrogen evolution, Electrochim. Acta 217 (2016) 156–162.
[44] J.L. Shi, J.M. Hu, Molybdenum sulfide nanosheet arrays supported on Ti plate: an efficient hydrogen-evolving cathode over the whole pH range, Electrochim. Acta 168 (2015) 256–260.
[45] J.J. Gao, P. Luo, H.J. Qiu, Y. Wang, Nanoporous FeP nanorods grown on Ti plate as an enhanced binder-free hydrogen evolution cathode, Nanotechnology 28 (2017) 105705.
[46] Z.H. Pu, Q. Liu, C. Tang, A.M. Asiri, X.P. Sun, Ni_2P nanoparticle films supported on a Ti plate as an efficient hydrogen evolution cathode, Nanoscale 6 (2014) 11031–11034.
[47] E.B. Carneiro-Neto, M.C. Lopes, E.C. Pereira, Simulation of interfacial pH changes during hydrogen evolution reaction, J. Electroanal. Chem. 765 (2016) 92–99.
[48] J.L. Lado, X.G. Wang, E. Paz, E. Carbo-Argibay, N. Guldris, C. Rodriguez-Abreu, L.F. Liu, K. Kovnir, Y.V. Kolen'ko, Design and synthesis of highly active Al-Ni-P foam electrode for hydrogen evolution reaction, ACS Catal. 5 (2015) 6503–6508.
[49] U.C. Lacnjevac, B.M. Jovic, V.D. Jovic, N.V. Krstajic, Determination of kinetic parameters for the hydrogen evolution reaction on the electrodeposited Ni-MoO_2 composite coating in alkaline solution, J. Electroanal. Chem. 677 (2012) 31–40.
[50] W. Sun, W. Wei, N. Chen, L. Chen, Y. Xu, C.J. Oluigbo, Z. Jiang, Z. Yan, J. Xie, In situ confined vertical growth of a 1D-$CuCo_2S_4$ nanoarray on Ni foam covered by a 3D-PANI mesh layer to form a self-supporting hierarchical structure for high-efficiency oxygen evolution catalysis, Nanoscale 11 (2019) 12326–12336.
[51] B. You, N. Jiang, M.L. Sheng, M.W. Bhushan, Y.J. Sun, Hierarchically Porous Urchin-Like Ni_2P Superstructures Supported on Nickel Foam as Efficient Bifunctional Electrocatalysts for Overall Water Splitting, ACS Catal. 6 (2016) 714–721.
[52] C. Tang, Z.H. Pu, Q. Liu, A.M. Asiri, Y.L. Luo, X.P. Sun, Ni_3S_2 nanosheets array supported on Ni foam: a novel efficient three-dimensional hydrogen-evolving electrocatalyst in both neutral and basic solutions, Int. J. Hydrogen Energy 40 (2015) 4727–4732.
[53] Y.H. Liang, X.P. Sun, A.M. Asiri, Y.Q. He, Amorphous Ni-B alloy nanoparticle film on Ni foam: rapid alternately dipping deposition for efficient overall water splitting, Nanotechnology 27 (2016) 12LT01.
[54] M. Fang, W. Gao, G.F. Dong, Z.M. Xia, S. Yip, Y.B. Qin, Y.Q. Qu, J.C. Ho, Hierarchical NiMo-based 3D electrocatalysts for highly-efficient hydrogen evolution in alkaline conditions, Nano Energy 27 (2016) 247–254.
[55] M. Zeng, Y.G. Li, Recent advances in heterogeneous electrocatalysts for the hydrogen evolution reaction, J. Mater. Chem. A 3 (2015) 14942–14962.
[56] Y.M. Shi, Y. Xu, S.F. Zhuo, J.F. Zhang, B. Zhang, Ni_2P Nanosheets/Ni Foam Composite Electrode for Long-Lived and pH-Tolerable Electrochemical Hydrogen Generation, ACS Appl. Mater. Interfaces 7 (2015) 2376–2384.
[57] N.N. Bai, Q. Li, D.Y. Mao, D.K. Li, H.Z. Dong, One-step electrodeposition of Co/CoP film on Ni foam for efficient hydrogen evolution in alkaline solution, ACS Appl. Mater. Interfaces 8 (2016) 29400–29407.
[58] J.M. Cao, J. Zhou, Y.F. Zhang, Y.X. Wang, X.W. Liu, Dominating role of aligned MoS_2/Ni_3S_2 nanoarrays supported on three-dimensional Ni foam with hydrophilic interface for highly enhanced hydrogen evolution reaction, ACS Appl. Mater. Interfaces 10 (2018) 1752–1760.
[59] L.B. Ma, Y. Hu, R.P. Chen, G.Y. Zhu, T. Chen, H.L. Lv, Y.R. Wang, J. Liang, H.X. Liu, C.Z. Yan, H.F. Zhu, Z.X. Tie, Z. Jin, J. Liu, Self-assembled ultrathin $NiCo_2S_4$ nanoflakes grown on Ni foam as high-performance flexible electrodes for hydrogen evolution reaction in alkaline solution, Nano Energy 24 (2016) 139–147.
[60] J. Lu, T.L. Xiong, W.J. Zhou, L.J. Yang, Z.H. Tang, S.W. Chen, Metal nickel foam as an efficient and stable electrode for hydrogen evolution reaction in acidic electrolyte under reasonable overpotentials, ACS Appl. Mater. Interfaces 8 (2016) 5065–5069.
[61] C.-C. Hou, Q.-Q. Chen, C.-J. Wang, F. Liang, Z. Lin, W.-F. Fu, Y. Chen, Self-supported cedarlike semimetallic Cu3P nanoarrays as a 3D high-performance Janus electrode for both oxygen and hydrogen evolution under basic conditions, ACS Appl. Mater. Interfaces 8 (2016) 23037–23048.
[62] B. Long, H. Yang, M. Li, M.-S. Balogun, W. Mai, G. Ouyang, Y. Tong, P. Tsiakaras, S.J. Song, Interface charges redistribution enhanced monolithic etched copper foam-based Cu_2O layer/TiO_2 nanodots heterojunction with high hydrogen evolution electrocatalytic activity, Appl. Catal. B-Environ. 243 (2019) 365–372.

[63] L. Yu, H. Zhou, J. Sun, F. Qin, F. Yu, J. Bao, Y. Yu, S. Chen, Z. Ren, Cu nanowires shelled with NiFe layered double hydroxide nanosheets as bifunctional electrocatalysts for overall water splitting, Energy Environ. Sci. 10 (2017) 1820–1827.
[64] S. Oh, H. Kim, Y. Kwon, M. Kim, E. Cho, H. Kwon, Porous Co-P foam as an efficient bifunctional electrocatalyst for hydrogen and oxygen evolution reactions, J. Mater. Chem. A 4 (2016) 18272–18277.
[65] Y. Xu, C. Zheng, S.B. Wang, Y.D. Hou, 3D arrays of molybdenum sulphide nanosheets on Mo meshes: efficient electrocatalysts for hydrogen evolution reaction, Electrochim. Acta 174 (2015) 653–659.
[66] I. Herraiz-Cardona, E. Ortega, V. Perez-Herranz, Impedance study of hydrogen evolution on Ni/Zn and Ni-Co/Zn stainless steel based electrodeposits, Electrochim. Acta 56 (2011) 1308–1315.
[67] J.M. Olivares-Ramirez, M.L. Campos-Cornelio, J.U. Godinez, E. Borja-Arco, R.H. Castellanos, Studies on the hydrogen evolution reaction on different stainless steels, Int. J. Hydrogen Energy 32 (2007) 3170–3173.
[68] K. Uosaki, G. Elumalai, H.C. Dinh, A. Lyalin, T. Taketsugu, H. Noguchi, Highly Efficient Electrochemical Hydrogen Evolution Reaction at Insulating Boron Nitride Nanosheet on Inert Gold Substrate, Sci. Rep. 6 (2016) 32217.
[69] A. Kiani, S. Hatami, Fabrication of platinum coated nanoporous gold film electrode: a nanostructured ultra low-platinum loading electrocatalyst for hydrogen evolution reaction, Int. J. Hydrogen Energy 35 (2010) 5202–5209.
[70] Y. Shen, A.C. Lua, J.Y. Xi, X.P. Qiu, Ternary platinum-copper-nickel nanoparticles anchored to hierarchical carbon supports as free-standing hydrogen evolution electrodes, ACS Appl. Mater. Interfaces 8 (2016) 3464–3472.
[71] C. Su, J.Y. Xiang, F.S. Wen, L.Z. Song, C.P. Mu, D.Y. Xu, C.X. Hao, Z.Y. Liu, Microwave synthesized three-dimensional hierarchical nanostructure CoS_2/MoS_2 growth on carbon fiber cloth: a bifunctional electrode for hydrogen evolution reaction and supercapacitor, Electrochim. Acta 212 (2016) 941–949.
[72] D.S. Kong, H.T. Wang, Z.Y. Lu, Y. Cui, CoSe2 nanoparticles grown on carbon fiber paper: an efficient and stable electrocatalyst for hydrogen evolution reaction, J. Am. Chem. Soc. 136 (2014) 4897–4900.
[73] N. Zhang, S.Y. Gan, T.S. Wu, W.G. Ma, D.X. Han, L. Niu, Growth control of MoS_2 nanosheets on carbon cloth for maximum active edges exposed: an excellent hydrogen evolution 3D cathode, ACS Appl. Mater. Interfaces 7 (2015) 12193–12202.
[74] A.L. Wang, J. Lin, H. Xu, Y.X. Tong, G.R. Li, Ni_2P-CoP hybrid nanosheet arrays supported on carbon cloth as an efficient flexible cathode for hydrogen evolution, J. Mater. Chem. A 4 (2016) 16992–16999.
[75] D. Chanda, J. Hnat, M. Paidar, J. Schauer, K. Bouzek, Synthesis and characterization of $NiFe_2O_4$ electrocatalyst for the hydrogen evolution reaction in alkaline water electrolysis using different polymer binders, J. Power Sources 285 (2015) 217–226.
[76] J.J. Duan, S. Chen, B.A. Chambers, G.G. Andersson, S.Z. Qiao, 3D WS_2 nanolayers@heteroatom-doped graphene films as hydrogen evolution catalyst electrodes, Adv. Mater. 27 (2015) 4234–4241.
[77] Z.C. Xiang, Z. Zhang, X.J. Xu, Q. Zhang, C.W. Yuan, MoS2 nanosheets array on carbon cloth as a 3D electrode for highly efficient electrochemical hydrogen evolution, Carbon 98 (2016) 84–89.
[78] D.M. Hou, W.J. Zhou, K. Zhou, Y.C. Zhou, J. Zhong, L.J. Yang, J. Lu, G.Q. Li, S.W. Chen, Flexible and porous catalyst electrodes constructed by Co nanoparticles@nitrogen-doped graphene films for highly efficient hydrogen evolution, J. Mater. Chem. A 3 (2015) 15962–15968.
[79] Y.F. Zhao, X.Q. Xie, J.Q. Zhang, H. Liu, H.J. Ahn, K.N. Sun, G.X. Wang, MoS_2 nanosheets supported on 3D graphene aerogel as a highly efficient catalyst for hydrogen evolution, Chem. Eur. J. 21 (2015) 15908–15913.
[80] Y.F. Zhang, L.Z. Zuo, L.S. Zhang, Y.P. Huang, H.Y. Lu, W. Fan, T.X. Liu, Cotton wool derived carbon fiber aerogel supported few-layered $MoSe_2$ nanosheets As efficient electrocatalysts for hydrogen evolution, ACS Appl. Mater. Interfaces 8 (2016) 7077–7085.
[81] S. Chen, J.J. Duan, Y.H. Tang, B. Jin, S.Z. Qiao, Molybdenum sulfide clusters-nitrogen-doped graphene hybrid hydrogel film as an efficient three-dimensional hydrogen evolution electrocatalyst, Nano Energy 11 (2015) 11–18.
[82] X. Xu, H.F. Liang, F.W. Ming, Z.B. Qi, Y.Q. Xie, Z.C. Wang, Prussian blue analogues derived penroseite (Ni, Co)S_x2 nanocages anchored on 3D graphene aerogel for efficient water splitting, ACS Catal. 7 (2017) 6394–6399.
[83] S.K. Park, D.Y. Chung, D. Ko, Y.E. Sung, Y. Piao, Three-dimensional carbon foam/N-doped graphene@MoS_2 hybrid nanostructures as effective electrocatalysts for the hydrogen evolution reaction, J. Mater. Chem. A 4 (2016) 12720–12725.
[84] H. Wang, Y.J. Cao, G.F. Zou, Q.H. Yi, J. Guo, L.J. Gao, High-performance hydrogen evolution electrocatalyst derived from Ni_3C nanoparticles embedded in a porous carbon network, ACS Appl. Mater. Interfaces 9 (2017) 60–64.
[85] M. Inagaki, T. Morishita, A. Kuno, T. Kito, M. Hirano, T. Suwa, K. Kusakawa, Carbon foams prepared from polyimide using urethane foam template, Carbon 42 (2004) 497–502.
[86] Z.K. Kou, T.T. Wang, Y. Cai, C. Guan, Z.H. Pu, C.R. Zhu, Y.T. Hu, A.M. Elshahawy, J. Wang, S.C. Mu, Ultrafine molybdenum carbide nanocrystals confined in carbon foams via a colloid-confinement route for efficient hydrogen production, Small Meth. 2 (2018) 1700396.
[87] Q.Q. Zhang, F. Zhang, S.P. Medarametla, H. Li, C. Zhou, D. Lin, 3D printing of graphene aerogels, Small 12 (2016) 1702–1708.
[88] X.L. Huang, S. Chang, W. Siang, V. Lee, J. Ding, J.M. Xue, Three-dimensional printed cellular stainless steel as a high-activity catalytic electrode for oxygen evolution, J. Mater. Chem. A 5 (2017) 18176–18182.
[89] B. Bian, D. Shi, X.B. Cai, M.J. Hu, Q.Q. Guo, C.H. Zhang, Q. Wang, A.X. Sun, J. Yang, 3D printed porous carbon anode for enhanced power generation in microbial fuel cell, Nano Energy 44 (2018) 174–180.
[90] A. Ambrosi, M. Pumera, Self-contained polymer/metal 3D printed electrochemical platform for tailored water splitting, Adv. Funct. Mater. 28 (2018) 1700655.
[91] H. Li, C. Tsai, A.L. Koh, L.L. Cai, A.W. Contryman, A.H. Fragapane, J.H. Zhao, H.S. Han, H.C. Manoharan, F. Abild-Pedersen, J.K. Norskov, X.L. Zheng, Activating and optimizing MoS_2 basal planes for hydrogen evolution through the formation of strained sulphur vacancies, Nat. Mater. 15 (2016) 48–53.
[92] M. Caban-Acevedo, M.L. Stone, J.R. Schmidt, J.G. Thomas, Q. Ding, H.C. Chang, M.L. Tsai, J.H. He, S. Jin, Efficient hydrogen evolution catalysis using ternary pyrite-type cobalt phosphosulphide, Nat. Mater. 14 (2015) 1245–1251.
[93] Y. Jiao, Y. Zheng, K. Davey, S.Z. Qiao, Activity origin and catalyst design principles for electrocatalytic hydrogen evolution on heteroatom-doped graphene, Nat. Energy 1 (2016) 16130.
[94] B. Yu, F. Qi, B.J. Zheng, W.Q. Hou, W.L. Zhang, Y.R. Li, Y.F. Chen, Self-assembled pearl-bracelet-like $CoSe_2$-$SnSe_2$/CNT hollow architecture as highly efficient electrocatalysts for hydrogen evolution reaction, J. Mater. Chem. A 6 (2018) 1655–1662.
[95] C.G. Hu, L.M. Dai, Multifunctional carbon-based metal-free electrocatalysts for simultaneous oxygen reduction, oxygen evolution, and hydrogen evolution, Adv. Mater. 29 (2017) 1604942.
[96] H.Y. Li, S.M. Chen, Y. Zhang, Q.H. Zhang, X.F. Jia, Q. Zhang, L. Gu, X.M. Sun, L. Song, X. Wang, Systematic design of superaerophobic nanotube-array electrode comprised of transition-metal sulfides for overall water splitting, Nat. Commun. 9 (2018) 2452.
[97] G. Feng, Y. Kuang, Y.J. Li, X.M. Sun, Three-dimensional porous superaerophobic nickel nanoflower electrodes for high-performance hydrazine oxidation, Nano Res. 8 (2015) 3365–3371.
[98] Q. Zhang, P.S. Li, D.J. Zhou, Z. Chang, Y. Kuang, X.M. Sun, Superaerophobic ultrathin Ni-Mo alloy nanosheet array from in situ topotactic reduction for hydrogen evolution reaction, Small 13 (2017) 1701648.
[99] J.L. He, B.B. Hu, Y. Zhao, Superaerophobic electrode with metal@metal-oxide powder catalyst for oxygen evolution reaction, Adv. Funct. Mater. 26 (2016) 5998–6004.
[100] M. Jiang, H. Wang, Y.J. Li, H.C. Zhang, G.X. Zhang, Z.Y. Lu, X.M. Sun, L. Jiang, Superaerophobic RuO_2-based nanostructured electrode for high-performance chlorine evolution reaction, Small 13 (2017) 1602240.